

The Photophysics of the Carrier of Extended Red Emission

Tracy L. Smith¹ & Adolf N. Witt²

ABSTRACT

Interstellar dust contains a component which reveals its presence by emitting a broad, unstructured band of light in the 540 to 950 nm wavelength range, referred to as Extended Red Emission (ERE). The presence of interstellar dust and ultraviolet photons are two necessary conditions for ERE to occur. This is the basis for suggestions which attribute ERE to an interstellar dust component capable of photoluminescence. In this study, we have collected all published ERE observations with absolute-calibrated spectra for interstellar environments, where the density of ultraviolet photons can be estimated reliably. In each case, we determined the band-integrated ERE intensity, the wavelength of peak emission in the ERE band, and the efficiency with which absorbed ultraviolet photons are contributing to the ERE. The data show that radiation is not only driving the ERE, as expected for a photoluminescence process, but is modifying the ERE carrier as manifested by a systematic increase in the ERE band's peak wavelength and a general decrease in the photon conversion efficiency with increasing densities of the prevailing exciting radiation. The overall spectral characteristics of the ERE and the observed high quantum efficiency of the ERE process are currently best matched by the recently proposed silicon nanoparticle (SNP) model. Using the experimentally established fact that ionization of semiconductor nanoparticles quenches their photoluminescence, we proceeded to test the SNP model by developing a quantitative model for the excitation and ionization equilibrium of SNPs under interstellar conditions for a wide range of radiation field densities. With a single adjustable parameter, the cross section for photoionization, the model reproduces the observations of ERE intensity and ERE efficiency remarkably well. The assumption that about 50% of the ERE carriers are neutral under radiation conditions encountered in the diffuse interstellar medium leads to a prediction of the ionization cross section of SNPs of average diameter of 3.5 nm for single-photon ionization of $\leq 3.4 \cdot 10^{-15} \text{ cm}^2$. The shift of the ERE band's peak wavelength toward larger values with increasing radiation density requires a

¹Department of Physics & Astronomy, Louisiana State University, Baton Rouge, LA 70803

²Ritter Astrophysical Research Center, The University of Toledo, Toledo, OH 43606

change of the size distribution of the actively luminescing ERE carriers through a gradual removal of the smaller particles by size-dependent photofragmentation. We propose that heat-assisted Coulomb decay of metastable, multiply charged SNPs is such a process, which will remove selectively the smaller components of an existing SNP size distribution.

Subject headings: dust: extended red emission: silicon nanoparticles, photo-physics

1. Introduction

Extended Red Emission (ERE) is an interstellar photoluminescence phenomenon, which is widely observed in astrophysical environments where interstellar dust is exposed to ultraviolet photons (Gordon et al. 1998, and references therein). The emission appears in the form of a broad, unstructured band, limited in extent to the 540 - 950 nm spectral range. The pronounced variability of the peak wavelength of this band (610 - 880 nm) and the correlated variability of the FWHM of the band (60 - 180 nm) are two defining characteristics of the ERE (Darbon et al. 1999). Recent summaries of the observational data concerning the ERE have been given by Witt et al. (1998), Smith (2000) and by Ledoux et al. (2001), which should be consulted for the numerous observational references.

The peak intensity of the ERE in different environments, ranging from the high-Galactic-latitude diffuse interstellar medium (ISM) of the Milky Way Galaxy to HII regions, is generally proportional to the density of the illuminating radiation field (Gordon et al. 1998). This is expected for a photon-driven process involving an interstellar dust mixture, in which the ERE carrier represents an approximately constant fraction of the dust mass. However, a high degree of spatial variability of the ERE intensity, e.g. the presence of bright ERE filaments contrasted by locations without any detectable ERE within the same individual objects, is also part of the ERE phenomenon (e.g. Witt & Malin 1989; Witt & Boroson 1990). While faintest on an absolute scale in the diffuse ISM of the Galaxy, the ERE, there, is comparatively intense relative to the density of the prevailing radiation field (Gordon et al. 1998; Szomoru & Guhathakurta 1998). The correlation of ERE intensity with HI column density at high galactic latitudes has led to an estimate of a lower limit to the quantum yield of the ERE process of 10 ± 3 % (Gordon et al. 1998). This lower limit was arrived at with the assumption that the ERE carrier is the sole source of absorption of interstellar photons in the 90 - 550 nm spectral range. Given that almost certainly other dust components contribute to this absorption, the intrinsic quantum efficiency of the ERE carrier must exceed the lower-limit estimate in inverse proportion to the fraction of photons actually absorbed

by it.

The realization that the ERE carrier is both a luminescing agent of high intrinsic quantum efficiency ($\gg 10\%$) as well as a major contributor to the UV/optical absorption by interstellar grains had a profound impact on the discussion over the identification of the ERE carrier's nature. If we estimate the intrinsic quantum yield to be about 50%, the ERE carrier intercepts about 20% of the photons absorbed by interstellar dust in the 90 - 550 nm range. In view of this high cross section, the ERE carrier is restricted chemically to the small number of relatively abundant but highly depleted elements making up most of the mass of interstellar grains, i.e. C, Fe, Si, Mg, plus O and H. Even without these new restrictions, many of the previously proposed ERE carrier candidates, which are laboratory analog materials and models, had encountered serious difficulties. Proposed candidates either lacked the ability to match the wide range of ERE spectral variations or they implied the presence of additional emission features or significant continuum luminescence shortward of 540 nm, which is not in agreement with observations. Witt et al. (1998) and Ledoux et al.(2001) present detailed discussions of proposed ERE carrier candidates and the shortcomings of most.

With the high intrinsic quantum efficiency added to the observational constraints, the discussion over viable ERE carrier candidates currently has narrowed to a choice between crystalline silicon nanoparticles (Ledoux et al. 1998; Witt et al. 1998; Ledoux et al. 2001) and aromatic hydrocarbon clusters (AHC) (Seahra & Duley 1999). The silicon nanoparticle (SNP) model derives its strength from the extensive agreement between laboratory-derived experimental data on SNP luminescence properties (e.g. Ledoux et al. 2000) and the astronomical ERE data, while relevant laboratory data for the AHCs currently do not exist for the size range of particles proposed by Seahra and Duley (1999). The AHC model, thus, is based upon theoretical extrapolations from smaller hydrocarbon molecules. Particular weaknesses of the AHC model include the relative constancy of the wavelength of its predicted emission peak (Seahra & Duley 1999, Fig. 2), its prediction of secondary features not confirmed by observation (Gordon et al. 2000), and a suggested correlation between the strength of absorption in the 217 nm UV extinction band and the intensity of the ERE, again at variance with observation.

By contrast, the SNP model can explain the variable peak wavelength of the ERE band through the size dependence of photoluminescence by oxygen-passivated silicon nanocrystals residing within the quantum-confinement regime (Delerue et al. 1993; Ledoux et al. 2000; Takeoka et al. 2000). Furthermore, the quantum efficiency of individual well-passivated SNPs has been found experimentally to be near 100% (Credo et al. 1999; Ledoux et al. 2001). The absorption coefficient per unit volume of nanocrystalline silicon (Theiss 1997; Li

& Draine 2001) is about an order of magnitude larger than that of average interstellar dust (Huffman 1977), so that the cosmic abundance of Si seems sufficient to explain the observed ERE intensities (Witt et al. 1998) and the required associated UV/optical absorption cross section. Ledoux et al. (2001) have estimated that the mass of interstellar SNPs would be about 2% of the mass of all interstellar dust, if the intrinsic quantum efficiency of interstellar SNPs is 50%. This would require about 20% of the interstellar silicon in the case that the relative abundance of silicon is given by solar abundances, but close to 40%, if B-star abundances prevail (Snow & Witt 1996). Furthermore, recent observations (Gordon et al. 2000) have revealed tentative evidence for the existence of a second, related luminescence band at $1.15 \mu\text{m}$ in a bright ERE filament in the reflection nebula NGC 7023, matching in wavelength and width a similar band seen in SNPs at low temperatures in the laboratory (Meyer et al. 1993; Takeoka et al. 2000). An increasingly compelling case can thus be made that SNPs may well be the carriers of the ERE, because their experimentally established properties meet the constraints imposed by ERE observations and cosmic abundances. However, new constraints based upon the expected infrared emission characteristics of SNPs (Li & Draine 2001) have been proposed recently, which, when combined with suitably sensitive observations, may soon place severe limits on the possible interstellar abundance of oxygen-passivated SNPs or of pure-silicon SNPs.

Both the AHC and the SNP models, just as earlier ERE models based on hydrogenated amorphous carbon solids, such as HAC (Duley 1985) or QCC (Sakata et al. 1992), rely on across-bandgap recombination of electrons and holes in a semiconductor structure for the source of emission in the ERE band. The width of the band, in all instances, is attributed to a distribution of sizes of the luminescent entities with size-dependent bandgaps, while the peak wavelength of the band is related to the bandgap of the dominant particle size. In this paper we plan to examine whether the photophysics of such semiconductor nanoparticles under astrophysical conditions can account for the characteristics of the ERE seen in a wide range of astrophysical environments. We will be guided by experimental results found for SNPs and other semiconductor nanoparticles, and we will use experimentally determined parameters for SNPs, where available, as input into numerical calculations.

First, however, we begin by characterizing the environments, where ERE has been observed. We compute the UV-radiation densities for these environments and compile data for the wavelengths of peak ERE intensities and band-integrated ERE intensities. We proceed by estimating ERE quantum yields for locations other than the diffuse ISM. Then, starting from a strong base of experimentally determined properties of SNPs, we develop a model for the photophysics of the ERE carrier in interstellar environments. This model must explain, in a self-consistent manner, the observed variations of the ERE intensity, the ERE quantum efficiency, and the ERE peak wavelength as a function of the density and hardness of the

local radiation fields. This model will identify the photoionization of the ERE carrier as the physical process which controls the fraction of carrier particles capable of luminescing in a given environment, which itself is characterized by the density and spectrum of the prevailing photons and by the density and temperature of the free electrons. Finally, this model must lend itself to making specific predictions both with respect to future ERE observations as well as to yet not-measured carrier properties.

In Section 2 of this paper, we accumulate the available observational data, which provide information on ERE intensities, ERE quantum efficiencies, and ERE-band peak wavelengths in different sources. Critical elements will be the estimates of the UV radiation densities and the lower limits to the ERE quantum efficiencies, which will be determined from information about the spectral types and luminosities of the illuminating stars, the projected distances of the observed regions from the sources in question, and the observed ratios of ERE intensity to scattered light intensity over the same wavelength band. In Section 3 we introduce evidence showing photoionization to be a possible process controlling the ERE; we discuss the ionization mechanisms and their respective rates, and we present the relevant rate equations and their solutions. Section 4 contains the discussion where observational data and model predictions will be compared. This is followed by a summary in Section 5.

2. The Intensity, Peak Wavelength, and Efficiency of ERE

2.1. Data and Observations

We restricted our data sample to objects and environments where the sources of illumination are well-known with respect to spectral type, distance, and luminosity, thus permitting a reliable estimate of the density of the exciting radiation field. Furthermore, we focused on objects where the dust compositions are derived from average interstellar dust rather than being the result of local dust formation. Thus, we excluded existing ERE observations of planetary nebulae (Furton & Witt 1990, 1992) and limited ourselves to reflection nebulae, HII regions, dark nebulae, and the diffuse, high- $|b|$ Galactic cirrus, all in the Milky Way Galaxy.

Twenty-one of the twenty-two reflection nebulae (RN) included here were observed by Witt & Boroson (1990) during a spectroscopic survey of RN, wherein the ERE band-integrated intensity and the peak wavelength of the ERE band were measured. For the Orion Nebula, these quantities were taken from the observations of Perrin & Sivan (1992). The data for the high-Galactic-latitude dark nebula Lynds 1780 (L 1780) were taken from the spectrophotometric observations of Mattila (1979). One observation of an ERE peak

wavelength for the Red Rectangle was obtained from Rouan et al. (1995) and one peak ERE wavelength point for the Bubble Nebula (NGC 7635) was taken from Sivan & Perrin (1993). The ERE peak wavelength measurement for a high-Galactic-latitude cirrus came from Szomoru & Guhathakurta (1998) and the efficiency and band-integrated intensity of ERE in the ISM were taken from Gordon et al. (1998).

2.2. Dependence of ERE Properties on Radiation Field

Gordon et al. (1998) demonstrated that in a multitude of ERE sources the ERE band-integrated intensities and the intensities of the scattered light in the same wavelength band are roughly proportional to each other over several orders of magnitude in intensity. The scattered light intensity is determined by the column density of scattering grains and the density of the illuminating radiation in the wavelength range of the ERE band. This finding, therefore, suggests that, on average, the ERE carriers represent a fixed fraction of the dust present and that the closely related illuminating radiation field at wavelengths shorter than the ERE band is the source of ERE excitation. To quantify this relationship, an estimate of the densities of the exciting radiation fields is essential.

An analysis of ERE intensity variations in reflection nebulae in relation to the degree of internal reddening as a function of position within these nebulae by Witt & Schild (1985) and the non-detection of ERE in reflection nebulae illuminated by stars cooler than 7000 K (Darbon et al. 1999; Witt & Rogers 1991) suggest that the excitation of the ERE carrier is dominated by photons in the wavelength range shortward of 250 nm. We estimated the relevant radiation field density in the diffuse ISM, U_{isrf} , by integrating over the flux values of Mathis et al. (1983) from 91 to 250 nm at a distance of 10 kpc from the Galactic Center. All other radiation field densities will be normalized to this reference value, $U_{isrf} = 9.7 \cdot 10^{-14}$ ergs cm⁻³.

Then, for nebulae with known illuminating stars, we calculated the radiation field density at the top of the illuminating star’s atmosphere, U_{star} , using the star’s temperature and the appropriate atmosphere model (Kurucz et al. 1974) for the wavelength range from 91 to 250 nm. This radiation field density was then corrected for geometric dilution,

$$U_{obs} = \frac{U_{star}}{2} \left(\frac{r}{D}\right)^2, \quad (1)$$

where U_{obs} is the radiation field density at the point of ERE observation, r is the stellar radius and D is the projected distance of the ERE observation from the star in the plane

of the sky. The radiation field strength for each point of observation was then expressed in units of U_{isrf} ,

$$U = \frac{U_{obs}}{U_{isrf}}. \quad (2)$$

Since the values of D are measured in the plane of the sky, they are lower limits to the true distances of the observed positions from the stars, and U is an upper limit to the actual radiation field strength. Figure 1 shows a plot of the accumulated ERE intensity values versus the associated densities of the radiation field within specific and among different RN, the Orion Nebula, L 1780, the diffuse ISM, and the Red Rectangle. The diffuse ISM point is an average of many lines of sight (Gordon et al. 1998). The downward-pointing error bars on some of the RN points indicate upper limit determinations for the ERE intensity by Witt & Boroson (1990). The Red Rectangle is included here to indicate its exceptional ERE brightness, but we note that the dust in this bi-polar proto-planetary nebula is most likely of local origin and thus is not representative of the typical interstellar dust mixture. Figure 1 confirms that the different ERE intensities in the diffuse ISM, in RN and in the Orion Nebula are a result of scaling the density of the exciting radiation fields, as expected for a photoluminescence process. Specifically, we expect the ERE intensity to exhibit a proportionality given by

$$I(ERE) \propto U \cdot \eta \cdot (1 - \exp(-\tau_{ERE})), \quad (3)$$

where η is the ERE photon conversion efficiency, defined in the following section, and where τ_{ERE} is the effective optical depth for dust absorption at the wavelength of the ERE. The examination of Figure 1 reveals that the detected ERE intensities range over four orders of magnitude, while the corresponding exciting radiation field densities vary by about six orders of magnitude. Given that the values of τ_{ERE} are comparable in the different ERE sources, Figure 1 provides the first qualitative evidence for substantial variations in the ERE efficiency among different environments. In particular, the Red Rectangle, illuminated by a relatively cool B 9.5 III star, must derive its exceptional ERE intensity, when compared with the more typical RN, from a combination of high intrinsic efficiency and relative overabundance of ERE carriers, most likely produced in the local mass outflow.

Figure 2 shows the relationship between ERE-band peak wavelength, λ_p , and radiation field density. Again, due to the projection effect, the radiation field strengths calculated for the RN, Orion Nebula, and the Red Rectangle are strict upper limits. Figure 2 indicates

that the longest peak wavelengths for the ERE band are found in high radiation density environments, and the shortest are found in the lowest radiation density environments, as represented by the high-Galactic-latitude cirrus. The high- $|b|$ dark nebula L 1780 appears to take on an outlier role. We will comment on the likely explanation for this effect in Sect. 4.3.

2.3. The Photon Conversion Efficiency of the ERE Process

One can estimate a lower limit to the ERE conversion efficiency, if both the number of emitted ERE photons and the number of UV/optical photons absorbed within the same environment are known. It is assumed that the photons absorbed by dust which can possibly lead to the emission of an ERE photon are in the wavelength range between 91 nm (ionization of H) and 540 nm (edge of ERE band), although 250 nm is probably a more realistic upper limit of this range (see Sect. 2.2). The efficiency determined in this manner is a lower limit only, because other dust components, which are not contributing to the ERE, may participate in the photon absorption and the ERE excitation may occur primarily in the short-wavelength portion of the assumed wavelength window of exciting radiation.

Spectroscopic observations of reflection nebulae show the ERE band superimposed on a scattered light continuum. The scattered intensity beneath the ERE band, $I_{sca}(\text{band})$, is a direct probe of the number of illuminating photons within the ERE band and the number of dust grains present in the observed volume giving rise to the ERE. Given the knowledge of (1) the illuminating star’s spectral energy distribution, which relates the number of illuminating and scattered photons in the ERE band to the number of photons capable of exciting the ERE, (2) the wavelength dependence of extinction and (3) the wavelength dependence of the dust albedo, the number of photons absorbed between 91 nm and 540 nm, $N_{abs}(91-540 \text{ nm})$, can be estimated. The photoluminescence efficiency can then be found as

$$\eta = \left(\frac{N_{ERE}}{N_{sca}(\text{band})} \right) \left(\frac{N_{sca}(\text{band})}{N_{abs}(91 - 540\text{nm})} \right) \quad (4)$$

where $N_{ERE}/N_{sca}(\text{band})$ is the ratio of the number of ERE photons and scattered photons, each integrated over all solid angles. This ratio is not observationally accessible to a spatially fixed observer. Instead, we measure the intensity ratio $I_{ERE}/I_{sca}(\text{band})$, which depends strongly on the range of the dominant scattering angles in a given nebula, defined by the unknown nebular geometry and the direction to the observer. The direction dependence of the intensity ratio is caused by the fact that the scattered light intensity is subject to a

highly asymmetric phase function, while the ERE is expected to be emitted isotropically. This expectation is supported by experimental evidence, showing colloidal SNPs to exhibit no polarization memory (Koch et al. 1996). Multiple phonon-exciton interactions during the long radiative lifetime of SNPs as well as the rapid rotation of free-flying SNPs effectively destroy all directional relations between exciting photons and emitted ERE photons. This assessment is confirmed by the observed ERE band intensities and the corresponding scattered light intensities seen in RN (Witt & Boroson 1990, Fig. 1). For a given scattered light intensity, the ERE intensities in RN vary by about one order of magnitude at most, while for a given ERE intensity the corresponding scattered light intensities vary by nearly two orders of magnitudes. We hope to overcome this basic problem by averaging over multiple observations in a given RN and by averaging the data for a relatively large sample of RN representing a range of geometries, and with this reservation set $N_{ERE}/N_{sca}(\text{band}) = I_{ERE}/I_{sca}(\text{band})$.

The ratio of photons scattered within the wavelength range of the ERE band to photons absorbed within the wavelength range 91 - 540 nm, $N_{sca}(\text{band})/N_{abs}(91-540 \text{ nm})$, was determined with the help of a Monte Carlo radiative transfer code. This code included the local dust opacity law, characterized by the value of the ratio of total to selective extinction, R_V , the wavelength dependence of the dust albedo and phase function, and the spectral energy distribution of the exciting star, characterized by its effective temperature. The principal source of uncertainty, again, is the unknown geometry of the RN, which can be different in each instance. For simplicity, we adopted a spherical geometry with a centrally embedded star. The optical depth of the radius (1 pc) was taken to be 0.5 at the ERE wavelength and the density of the nebulae was assumed uniform. The absolute surface brightness and radial surface brightness distribution produced with such models agree well with measured surface brightness data for bright reflection nebulae (Witt & Schild 1986). In the model output, we examined the ratio $N_{sca}(\text{band})/N_{abs}(91 - 540 \text{ nm})$ at an intermediate angular offset corresponding to 0.3 of the projected radius of the nebula. This arrangement covers a large range of scattering angles but still favors forward-scattering, appropriate for a collection of objects which include many of the RN with the highest-known surface brightnesses. Calculations were performed for two values of the UV albedo, 0.4 and 0.6, to correspond to limiting cases of low R_V /strong 218 nm absorption feature and high R_V /weak 218 nm absorption feature, respectively. The dust albedo in the ERE band was set at 0.6, consistent with numerous observational determinations (Witt & Gordon 2000). The phase function asymmetry was assumed to increase with decreasing wavelength, e.g., $g = 0.6$ at the ERE wavelength vs. $g = 0.7$ at the wavelength of the exciting UV radiation. An example of the model results for the ratio

$$\frac{I(ERE)}{I_{sca}(\text{band})} = \eta \cdot \frac{N_{abs}(91 - 540\text{nm})}{N_{sca}(\text{band})} \quad (5)$$

is shown for $\eta=0.01$ as a contour plot in Figure 3, for $a_{UV}=0.6$, $2.5 \leq R_V \leq 5.0$, and $1 \cdot 10^4\text{K} \leq T_{\text{eff}} \leq 3.5 \cdot 10^4\text{K}$, corresponding to stars of approximate spectral types A 0 to O 7. Figure 3 illustrates the fact that I_{ERE}/I_{sca} can change easily over a factor of 30 to 40 for the same value of the quantum efficiency η , depending upon the values of R_V and T_{eff} . Correct estimates for the nebular opacity law and the spectral type of the illuminating stars are, therefore, of critical importance. Table 1 shows the values we adopted for the nebulae with ERE detections and well-determined upper limits.

The uncertainties introduced by the range in UV dust albedos depend on the temperature of the illuminating stars and range from 15% to 25% for stars ranging from late B to late O spectral type. The uncertainties go in the direction of increasing the efficiency for a given ratio $I_{ERE}/I_{sca}(\text{band})$ for a higher UV albedo. While the overall uncertainties of the derived efficiencies for individual RN observations are difficult to assess for reasons discussed above, we estimate the uncertainty of the efficiency of the *average* of all RN detections to be about a factor of two.

The estimated efficiencies, as defined above, are plotted in Figure 4 as a function of the UV radiation density. The highest efficiencies found are associated with the lowest radiation densities. Also, among reflection nebulae, illuminated by stars between spectral types A 0 and B 0, we note a significant decline of the ERE efficiency by about two orders of magnitude as the radiation density increases by a similar factor. The Orion Nebula data do not follow this general trend, a fact that needs to be explained by our model (*c.f.* Sect. 3.4). We do not include the Red Rectangle data in this graph, because the dust mixture in this object is not derived from interstellar dust but is locally produced. We will discuss the efficiency of the ERE carriers in the Red Rectangle below.

2.4. The Red Rectangle

The Red Rectangle occupies a special role in the problem of understanding the ERE. Given the relatively cool illuminating star in the object, the exceptionally high ERE intensity suggests that the ERE carriers are present here with an unusually high relative abundance, most likely as a result of local production. By employing the same method as used for RN, we estimate an efficiency for the photon conversion of $\sim 20\%$, the highest value seen in any object. The principal source of uncertainty here is the unusual opacity law characterizing the

Table 1: Data Related to Efficiency Estimates

Object	Star Sp. T.	R_V	$I_{ERE}/I_{sca}(\text{band})$	$\eta(\%)$
NGC 1333	B8 V	4.7	0.07 - 0.16	1.8 - 4.0
NGC 1788	B9 V	4	< 0.03	< 1.04
NGC 1999	A0	~ 3.6	0.06	2.0
NGC 2068	B2 II - III	4	< 0.03	< 0.16
NGC 2023	B1.5 V	4.11	0.02 - 0.42	0.04 - 1.2
NGC 2071	B5 V	4.5	< 0.1	< 1.2
NGC 2247	B3 Pe	3.25	0.08	0.4
NGC 2327	B1	3.1 - 4.5	0.06	0.1
NGC 7023	B3 Ve	3.2	0.04 - 0.15	0.2 - 0.6
IC 59	B0 V	3.5	< 0.16	< 0.19
IC 63	B0 IVe	~ 3.5	0.68	4.7
IC 348	B5 V	3.5	< 0.05	< 0.4
IC 426	B8 p	~ 4	0.21	7.9
IC 435	B5 V	5.3	< 0.01	< 0.13
IC 5076	B8 Ia	3.2	< 0.09	< 2.48
CED 167	B6 V	3.2	< 0.01	< 0.13
CED 201	B9.5 V	3.42	0.02	0.5
Maja	B7 III	3.2	< 0.02	< 0.32
Merope	B6 IV	3.6	< 0.01	< 0.01
VdB 132	B3 V	4	< 0.02	< 0.08
Orion Neb.	06, 07, 2xB0	5.5	0.20 - 0.64	0.4 - 1.3
L1780	ISRF	3.1	0.6	13
ISM	ISRF	3.1	0.2 - 2	10

matter in the Red Rectangle (Sitko et al. 1981), which is unlike that of any interstellar or nebular dust. There is only a very weak indication of absorption at the interstellar extinction band centered at 217.5 nm, but massive absorption shortward of 180 nm is present instead. The ERE is strongest along the X-shaped walls of the bi-polar outflow cone (Schmidt & Witt 1991), while the unidentified infrared band (UIB) at 3.3 μm is found to be weak to non-existent along the walls or interface areas, but very strong in the dust ring surrounding the central binary star (Kerr et al. 1999). Additionally, all of the remaining UIBs at 6.2, 7.7, 8.6 and 11.3 μm have been observed in the Red Rectangle (Russell et al. 1978). Waters et al. (1998) have used observations from the Infrared Space Observatory (ISO) to confirm the existence of crystalline silicates in a circum-binary disk in the nebula, which suggests a mixed chemistry for this object.

3. The Photoionization of Semiconductor Nanoparticles Under Astrophysical Conditions

3.1. The Silicon Nanoparticle Model

Before discussing the photoionization of semiconductor nanoparticles in general, it is essential to briefly summarize the main characteristics of the SNP model as representative of a possible carrier of the ERE. Silicon is an indirect-bandgap semiconductor material with a bandgap energy of 1.17 eV at 0 K. The indirect-bandgap nature implies that an excited electron located in the conduction band needs to undergo a change in momentum state before it can recombine with a hole in the valence band. This process, which involves electron-phonon interactions, has a long time constant ($\sim 10^{-5}$ - 10^{-3} s; Takeoka et al. 2000). Consequently, in the absence of spatial confinement and with an abundance of non-radiative recombination routes available in bulk silicon, photoluminescence in bulk crystalline silicon is a highly unlikely process. Several important changes occur when a transition to nanocrystals of silicon is considered (Freedhoff & Marchetti 1997). First, size-dependent quantum confinement of the electron-hole exciton causes the bandgap to widen, shifting it from 1.17 eV to values consistent with the wavelength range of the ERE band (Ledoux et al. 2000). Second, the spatial confinement of the electron forces its wavefunction to spread in momentum space in accordance with the Heisenberg uncertainty principle, greatly enhancing the probability of radiative recombination with the hole in the valence band without phonon collisions. Thus, efficient photoluminescence at energies much higher than 1.17 eV becomes possible. However, this occurs only, provided that all dangling Si bonds at the surface of the nanocrystal are passivated, e.g., by hydrogen or oxygen atoms. Observational constraints suggest that interstellar Si nanocrystals would be passivated by oxygen (Witt et al. 1998).

For a range of diameters from 1 nm to 7 nm, the peak energy of photoluminescence of SNPs varies between 1.9 eV and 1.2 eV (Takeoka et al. 2000), in agreement with the wavelength range over which ERE has been observed in astronomical sources. And third, the small size of the nanocrystal makes it much easier to arrive at a defect-free structure. The presence of defects would otherwise provide for radiationless recombination routes, which would be detrimental to a high quantum efficiency. As a consequence, the resulting well-passivated, nanocrystalline system is a particle capable of photoluminescence with essentially 100% efficiency, emitting a luminescence photon upon each excitation by a photon with an energy exceeding that of the bandgap of the particle in question (Credo et al. 1998). An appropriate size distribution of such particles can then account for the observed interstellar luminescence seen as ERE, provided suitable shorter-wavelength photons are present to cause the excitation.

Secondary, but equally important, aspects of the SNP model concern a plausible mode of formation under astrophysical conditions and adequate cosmic abundance of silicon to explain the observed ERE intensities. Witt et al. (1998) suggested that the formation of interstellar SNPs could occur as a result of the nucleation of SiO molecules in oxygen-rich stellar outflows (Castro-Carrizo et al. 2001; Roche et al. 1991; Hirano et al. 2001; Garray et al. 2000; Zhang et al. 2000; Rietmeijer et al. 1999; Gail & Sedlmayr 1999). To lead to SNPs, the nucleation of SiO must be followed by annealing and phase separation into an elemental silicon phase in the core and a passivating mantle of SiO₂. In fact, the SiO₂ phase is thermodynamically more favorable for solid silicon oxides. Recent experiments involving the evaporation and recondensation of SiO lend strong support to this suggestion (Rinnert et al. 1998, 1999; Murakami et al. 1998). The nucleation of SiO molecules is a proposed first stage of the formation of silicate grains (Gail & Sedlmayr 1999), although the theoretical understanding of this formation process is still far from complete. Given the high mass absorption coefficient of nanocrystalline silicon (Theiss 1997) and the high quantum efficiency of SNPs, it has been estimated that the mass of interstellar SNPs amounts to only 1% to 2% of the interstellar dust mass (Ledoux et al. 2001), while silicon contributes about 8% of the total mass of interstellar solids condensed from a gas of solar composition (Whittet 1992, p.52).

The absorption of interstellar photons by SNPs occurs primarily in the mid- and far-ultraviolet (Zubko et al. 1999; Theiss 1997), which is consistent with astronomical assessments of the excitation of the ERE (Witt & Schild 1985; Darbon et al. 1999). The expected oxide coating of SNPs not only is essential for effective passivation, assuring a high overall photoluminescence efficiency, it also contributes to the interstellar Si-O stretch absorption band at 9.7 μm and to a possibly prominent emission feature at 20 μm (Li & Draine 2001). Also, the oxide coating assures that even the smallest SNPs do not luminesce shortward of

540 nm by creating surface-related electronic states within the growing band gap of such particles (Wolkin et al. 1999). Finally, given that only about 25% of the energy of an absorbed typical ultraviolet photon is used to power the ERE, the bulk of the absorbed energy goes towards heating the SNPs (Duley 1992; Li & Draine 2001). As a consequence of the small size of the SNPs, temperature fluctuations may raise the temperatures of the particles temporarily into the range from 50 K to 300 K (Li & Draine 2001), causing them to contribute to thermally driven band and continuum dust emission, mainly in the 15 - 60 μm wavelength region.

3.2. Photoionization Control of ERE Carrier Photoluminescence

The observational data summarized in Sect. 2 strongly suggest that the ultraviolet photon field present in different ERE sources not only powers the ERE (Figure 1), but also controls the size distribution of luminescing particles (Figure 2) and the fraction of absorbing particles capable of luminescing (Figure 4). Two mechanisms must be considered: (i) partial, size-dependent photodestruction and (ii), size-dependent quenching of the photoluminescence by photoionization. Typical SNPs with spectra matching those of the ERE have between 200 and 6000 silicon atoms and their instantaneous photodestruction by thermal heating is a very unlikely process. The maximum temperatures of SNPs in typical ERE sources predicted by Li & Draine (2001) are in the 300 K - 500 K range for SNPs with diameters of 2nm, which is too low for thermal evaporation. An alternative process is fragmentation by Coulomb explosions of multiply charged SNPs. Such fragmentation, mostly by ejection of singly-charged monomers and dimers, has been seen experimentally in multiply-ionized, free silicon nanoparticles by Ehbrecht & Huisken (1999) and Bescos et al. (2000). It is not known, how the presence of an oxide shell affects this disintegration process. However, there is considerable experimental evidence that single ionization of semiconductor nanocrystals, including SNPs, effectively quenches their photoluminescence (Nirmal & Brus 1999; Banin et al. 1999; Efros & Rosen 1997; Nirmal et al. 1996; Kharchenko & Rosen 1996; Wang et al. 2001). If an ionized nanocrystal is photoexcited, the photogenerated electron-hole pair recombines by transferring its energy to the strongly Coulomb-coupled second hole via a non-radiative Auger decay process (Nirmal & Brus 1999). Partial ionization of SNPs is expected under conditions existing in the diffuse ISM and a higher degree of ionization, including multiple ionization, is expected in regions of higher radiation density (Bakes & Tielens 1994; Weingartner & Draine 2001). The threshold for single-photon ionization of free silicon clusters with about 200 silicon atoms has been found experimentally to lie near 5.1 eV (Fuke et al. 1993). We expect the ionization to be more difficult, if not requiring a higher energy, when a passivating oxide shell is present, but no experimental data appear to

exist for this case. The energy per exciting photon of most laboratory photoluminescence experiments is less than the ionization threshold value. Consequently, the ionization process usually seen under laboratory conditions is Auger ionization (Chepic et al. 1990; Kovalev et al. 2000b), which arises when a second electron is excited into the conduction band before the first electron has completed its recombination with its hole and when the combined excitation energies of the two electrons exceed the ionization threshold. The strong Coulomb interaction between the two excited electrons causes one to recombine with a hole while the other leaves the system. The Auger process is both highly efficient in quantum-confined nanocrystals, and particularly important in SNPs as a result of the long photoluminescence lifetime of singly-excited electrons residing in the conduction band, which ranges up to msec in duration, but is dependent on size and temperature of the SNPs (Takeoka et al. 2000).

Under interstellar conditions, the photon spectrum extends to 13.6 eV, and photoionization by single photons must clearly be the dominant process in the diffuse ISM, given the high degree of dilution of the interstellar radiation field. As we will show below, despite the fact that the rate of the two-photon Auger ionization process increases with the square of the radiation field density, the two ionization processes are not likely to reach comparable rates in any of the radiation environments, where ERE is observed.

As shown in Figure 4, the observed lower limit of the ERE quantum yield in the diffuse ISM is about 10 ± 3 % (Gordon et al. 1998). After making allowance for other grain components contributing to the absorption of UV/optical photons without contributing to the ERE, we may estimate that the intrinsic quantum efficiency of the ERE carrier particles could be near 50% (Witt et al. 1998). If photoionization controls the ability of the ERE carrier to luminesce, the intrinsic quantum efficiency then is proportional to the non-ionized fraction of the carrier particles. Thus, we find that the degree of ionization of the ERE carrier particles in the diffuse ISM must be fairly low, not exceeding 50%. The degree of ionization could be less, if a certain fraction of the carriers is otherwise defected and thus unable to luminesce, because the structure of such defected nanoparticles permits radiationless recombination of electrons and holes. These expectations regarding the ionization state of nm-sized ERE carrier particles are in good agreement with the predictions of likely charge states for particles of 3 nm diameter in the cold, diffuse ISM by Bakes & Tielens (1994) and Weingartner & Draine (2001)

The expected low degree of ionization in interstellar space places a strict upper limit on the ionization cross section of SNPs for single-photon ionization, assuming that SNPs cause the ERE. We will calculate this cross section below. Since no measurements exist for this cross section, our calculation will represent a specific prediction made by the SNP model, which later laboratory experiments may test.

3.3. The Photoionization Equilibrium Rate Equations and their Solutions

Let us assume that interstellar SNPs are perfectly passivated and that the only way to quench their photoluminescence is by photoionization. We further assume the absorption characteristics of SNPs to be unchanged, whether or not the latter are ionized. Then, under interstellar conditions, the photoluminescence properties of SNPs are controlled by the probabilities of occupation of four distinct states. The first is P_0 , the probability that a SNP is in the neutral ground state, with all electrons in the valence band. It is seen easily that P_0 measures the intrinsic photoluminescence quantum efficiency of the total SNP ensemble, consisting of neutral and ionized particles. The second essential probability is P_1 , which measures the fraction of SNPs in the neutral, excited state in which one electron is momentarily in the conduction band. Since the decay from this state almost invariably is via the emission of a photoluminescence photon, P_1 is directly proportional to the ERE intensity produced by the SNPs. A third state, measured by the probability P_2 , represents neutral SNPs in which a second photoexcitation has occurred before the first excitation had enough time to decay. The most likely result of the strong Coulomb interaction of the two electrons is Auger ionization on a timescale of typically $\tau_A \sim 10^{-10}$ s (Delerue et al. 1998), rendering the SNP unable to luminesce. However, under astrophysical conditions this probability is expected to be very small. The fourth state of importance is the ionized state, measured by the probability P_+ . SNPs can enter this state via either one of the two ionization processes. We will consider only the once-ionized state here, although multiply-ionized SNPs are likely in environments with high photon densities and comparatively low densities of free electrons. We ignore the possibility of negatively charged SNPs, because the rate of photoionization of negatively charged SNPs is expected to be large compared to the electron capture rate of a neutral SNP, given the radiation and electron densities in ERE-emitting environments. Our model accounts for the presence of higher positive charge states by increasing the value of τ , the lifetime of the ionized state. We will discuss the role of multiple ionization in SNPs in Section 3.5 of this paper.

We can formally express the time rate of change of the four probabilities P_0, P_1, P_2 , and P_+ , by the following rate equations (Chepic et al. 1990):

$$\dot{P}_0 = -W_1 \cdot P_0 - \frac{P_0}{\tau_i} + \frac{P_1}{\tau_1} \quad (6)$$

$$\dot{P}_1 = W_1 \cdot P_0 + \frac{P_2}{\tau_2} - \frac{P_1}{\tau_1} - W_2 \cdot P_1 + \frac{P_+}{\tau} \quad (7)$$

$$\dot{P}_2 = W_2 \cdot P_1 - \frac{P_2}{\tau_2} - \frac{P_2}{\tau_A} \quad (8)$$

$$\dot{P}_+ = \frac{P_2}{\tau_A} + \frac{P_0}{\tau_i} - \frac{P_+}{\tau} \quad (9)$$

and, consistent with our assumptions, the following normalization:

$$P_0 + P_1 + P_2 + P_+ = 1.0 \quad (10)$$

To solve these equations for any given environment, we assume steady state:

$$\dot{P}_0 = \dot{P}_1 = \dot{P}_2 = \dot{P}_+ = 0 \quad (11)$$

The factors W_1 and W_2 , respectively, represent the rates of photoexcitation of SNPs in the neutral ground state and the neutral, once-excited state by the prevailing radiation field, such that the combined energy of the two photons causing the excitations exceeds the ionization potential of the SNPs. For our subsequent calculations we will assume $W_1 = W_2$, which is approximately correct (Efros & Rosen 1997), given the ionization potential (Fuke et al. 1993) and typical bandgaps of SNPs. The lifetimes appearing in Equations (6) through (9) are: τ_1 , the radiative lifetime of the singly-excited state; τ_2 , the radiative lifetime of the doubly-excited state; τ_A , the lifetime of the doubly-excited state against Auger ionization; τ_i , the lifetime of the neutral state against photoionization by single photons; and τ , the lifetime of the ionized state before recapture of a free electron, leading to a return to the neutral state. We assume that the recaptured electron will appear in the conduction band of the SNP, with subsequent radiative transition to the valence band.

The solutions of Equations (6) through (11) are given by the following four expressions:

$$P_0 = \left[1 + \tau_1 \left(W_1 + \frac{1}{\tau_i} \right) + \frac{W_2 \tau_1 \left(W_1 + \frac{1}{\tau_i} \right)}{\left(\frac{1}{\tau_2} + \frac{1}{\tau_A} \right)} + \tau \left(\frac{W_2 \tau_1 \left(W_1 + \frac{1}{\tau_i} \right)}{\tau_A \left(\frac{1}{\tau_2} + \frac{1}{\tau_A} \right)} + \frac{1}{\tau_i} \right) \right]^{-1} \quad (12)$$

$$P_1 = \tau_1 \left(W_1 + \frac{1}{\tau_i} \right) \cdot P_0 \quad (13)$$

$$P_2 = \frac{\tau_1 W_2 \left(W_1 + \frac{1}{\tau_i} \right)}{\left(\frac{1}{\tau_2} + \frac{1}{\tau_A} \right)} \cdot P_0 \quad (14)$$

$$P_+ = \tau \left[\frac{\tau_1 W_2 \left(W_1 + \frac{1}{\tau_i} \right)}{\tau_A \left(\frac{1}{\tau_2} + \frac{1}{\tau_A} \right)} + \frac{1}{\tau_i} \right] \cdot P_0 \quad (15)$$

The ionization rate per SNP for single-photon ionization can be found from P_0/τ_i , while the 2-photon Auger ionization rate becomes P_2/τ_A . These two rates equal each other, provided

$$\tau_1 = \frac{\left(\tau_A \left(\frac{1}{\tau_2} + \frac{1}{\tau_A} \right) \right)}{\tau_i W_2 \left(W_1 + \frac{1}{\tau_i} \right)}. \quad (16)$$

3.4. Numerical Solutions

For the numerical evaluations of these solutions, we need to find values for the rate coefficients and time constants involved in Equations (12) through (15). We adopt the direction-integrated intensity of the interstellar radiation field at the galactocentric distance of the Sun given by Mathis et al. (1983) and the optical absorption cross sections of SNPs by Kovalev et al. (2000a), extrapolated into the ultraviolet, to estimate the radiative excitation rate in the diffuse interstellar medium. We find $W_1 \simeq 1.0 \cdot 10^{-5} \text{s}^{-1}$ for nanoparticles with diameters near 3.5 nm under these conditions, and, as discussed above, we set $W_1 = W_2$. The timescale τ for recombinations between ionized SNPs and free electrons is estimated from the work of Draine & Sutin (1987). With a characteristic diameter of 3.5 nm for a SNP with a single positive charge, an average electron density of $n_e = 0.03 \text{ cm}^{-3}$ from pulsar dispersion measures (Spitzer 1978), and an electron temperature $T_e = 100 \text{ K}$ we find $\tau \simeq 1.0 \cdot 10^6 \text{ s}$, which includes an enhancement of the particle cross section due to Coulomb focussing by a factor of about 200. The timescale for single-photon ionization, τ_i , cannot be estimated directly in the absence of measured ionization cross sections. However, the observation of a large ERE efficiency in the diffuse ISM suggests a fairly high ratio of neutral to ionized SNPs in this environment, and we estimate that $P_0 \sim 0.5$. Equation (12) then leads to the conclusion that $\tau_i \simeq 1.0 \cdot 10^6 \text{ s}$ for the diffuse ISM. Since single-photon ionization is the dominant photoionization process of SNPs in the diffuse ISM, we will use this result to estimate the cross section for this process later in Sect. 4.2. Moreover, as the radiation density increases, the single-photon ionization rate $\frac{1}{\tau_i}$ as well as the photoexcitation rates W_1 and W_2 scale in direct proportion of the radiation density. The radiative lifetime of the once-excited state, τ_1 , is strongly dependent upon size and temperature of the SNP and relatively long, consistent with the indirect-bandgap nature of silicon. From Takeoka et al. (2000) we estimate $\tau_1 = 2 \cdot 10^{-3} \text{ s}$ for an appropriate average. The dynamics of the doubly-excited state is controlled by the small value of $\tau_A \sim 10^{-10} \text{ s}$ (Efros & Rosen 1997). We will assume that radiative decay from the doubly-excited state is not entirely prohibited by setting $\tau_2 = 10^{-6} \text{ s}$.

We computed the probabilities P_0, P_1, P_2 and P_+ for a range of radiation densities extending from the interstellar density to $1 \cdot 10^6$ times the interstellar value. We also varied the lifetime of the ionized state, τ , from the interstellar value to $1 \cdot 10^6$ times shorter, in steps of factors of ten. τ scales in inverse proportion to the electron density when the single-charge state is the dominant state among ionized SNPs, but τ can be much longer than expected, if the bulk of SNPs are multiply ionized. At low electron energies, τ is relatively independent of the electron temperature (Draine & Sutin 1987), as the temperature dependences of electron velocity and recombination cross section cancel one another. Aside from a constant factor, which measures the unknown fraction of the SNP absorption to the total absorption

by all interstellar grains, the probability P_0 measures the intrinsic ERE quantum efficiency. Similarly, the probability P_1 is directly proportional to the ERE intensity. Finally, the ratios $\frac{P_0}{\tau_i}$ and $\frac{P_2}{\tau_A}$ measure the rates of single-photon ionization and two-photon Auger ionization, respectively.

In Figure 5 we plot the probability P_1 as a function of the radiation field density superimposed upon our ERE intensity data, compiled in Section 2. The model curves are normalized to fit the ERE intensity in the diffuse ISM at $\log(U) = 0$. The model provides a consistent explanation for all observed ERE intensities and upper limits by suggesting that the more intense radiation fields in reflection nebulae and HII regions will lead to higher ERE intensities, as long as the resultant increased photoionization rate is at least partially balanced by increased electron capture rates. The model fit suggests that in reflection nebulae the rate of returning ionized SNPs to the neutral state is up to one order of magnitude higher than in the diffuse ISM, consistent with the increased densities and the absence of hydrogen ionization in these objects. In the Orion Nebula, electron capture rates higher by at least five orders of magnitude than in the ISM are expected, consistent with electron temperatures of $T_e \sim 10^4$ K and electron densities near 10^4 cm^{-3} generally quoted for the Orion Nebula (Rubin et al. 1998; Baldwin et al. 1996). However, Figure 5 shows that the rate of returning ionized SNPs to the neutral state, $\frac{1}{\tau}$, increases by only three orders of magnitude between the ISM and the Orion Nebula. We attribute this smaller than expected increase to the dominance of multiple charge states among ionized SNPs in the Orion Nebula (Weingartner & Draine 2001; Bakes & Tielens 1994). Thus, most electron captures by ionized SNPs involve transitions between different charge states instead of transitions between the singly-charged state and the neutral state. It is of interest to note that only a fraction of about 1% neutral SNPs is needed in order to fit both the reflection nebulae and Orion Nebula intensity data. Despite this low fraction of SNPs capable of luminescing, the ERE intensities are nevertheless high, because (see Equation 3) the increase in the radiation field densities (factors of 10^3 to 10^5) more than balance the decrease in the efficiency (factor of ~ 50). In the Orion Nebula, a neutral SNP luminesces approximately once per second, while in the diffuse ISM only one luminescence event per neutral SNP occurs every 30 hours, on average.

In Figure 6 we plot the probability P_0 as a function of the radiation field density superimposed upon our ERE efficiency data produced in Section 2. Again, the model curves are normalized to fit the derived ERE efficiency for the diffuse ISM. The model matches the precipitous decline of the ERE quantum efficiency seen in reflection nebulae in the range $2 < \log(U) < 4$ exceedingly well. With the illuminating stars in reflection nebulae having spectral types B 1 V or later, these nebulae, with H and He in the neutral state, form a sequence of low-electron-density environments. The Orion Nebula, by contrast, maintains a

comparatively high ERE quantum efficiency, because its higher electron density effectively balances the ionizing effect of the more intense radiation upon the SNPs. The geometry of the Orion Nebula does not permit a reliable determination of whether the observed ERE in this object is produced in the ionized region or in the PDR on the face of the molecular cloud. However, the spatial distribution of the ERE detected in the HII region Sh 152 (Darbon et al. 2000) suggests a close association of the ERE with the ionized volume.

The comparison of the two SNP ionization processes is shown in Figure 7, where the predicted ionization rates per SNP are plotted as a function of the radiation field density. Two sets of curves are shown for values of the parameter τ differing by five orders of magnitude. Since the recombination of ionized SNPs with free electrons is independent of how a SNP was ionized, the ratio of the two ionization rates is dependent only upon the radiation density and not on τ . We find that the single-photon ionization process clearly is dominant under all conditions of radiation density found in the ERE sources studied here. For the two-photon Auger process to become important under interstellar conditions, the lifetime of the excited state in SNPs, τ_1 , would need to be increased from the experimentally observed value by about 3 orders of magnitude, i.e $\tau_1 \simeq 2$ s.

3.5. The Size-Dependence of the Ionization Equilibrium

The ERE band exhibits a considerable width, which is interpreted by the the SNP model as reflecting the size distribution of the actively luminescing particles. The observations of the shift of the peak of the ERE intensity toward longer wavelengths with increasing radiation density (Figure 2), when combined with the relationship between particle size and luminescence wavelength imposed by quantum confinement (Ledoux et al. 1998, 2000), imply that this active size distribution is progressively eroded by radiation, starting with the smallest particles. While the single-photon ionization cross section has yet to be measured, we expect that it is large enough to make single-photon ionization of SNPs dominant over two-photon Auger ionization under astrophysical conditions (Figure 7). We expect the size dependence of single-photon ionization of SNPs to involve a scaling with the geometric cross section $\sim a^2$, despite the fact that for particles with radius $a \ll \lambda$, the photon absorption cross section $C_{abs} \sim a^3$ (Bohren & Huffman 1983, p. 140). The reason for this difference lies in the fact that electron escape lengths are small compared to the diameter range of the SNPs assumed responsible for the ERE (Weingartner & Draine 2001). Ionization experiments with single 193 nm (6.4 eV) photons on neutral silicon nanocrystals (Ehbrecht & Huisken 1999) have demonstrated the preferential ionization of the larger nanoparticles in a given, narrow, size distribution, covering the cluster size range from 1000 to 2000 atoms. According to Fuke

et al. (1993), silicon clusters with more than 200 atoms have a first-ionization potential essentially equal to that of bulk silicon. Thus, the preferred ionization of larger clusters is not a result of a lower ionization potential. Therefore, if single-photon ionization is the only process considered as controlling the size distribution of actively luminescent SNPs, we conclude that the peak emission should shift progressively toward *shorter* wavelengths with increasing radiation density as a result of the preferential ionization of larger particles, the opposite of what is being observed.

If the SNP model is to be maintained, other radiation-driven processes must become important in high-radiation-density environments, which lead to the efficient elimination of the smallest SNPs. We propose that photofragmentation of multiply-charged SNPs, combined with single-photon heating, could be such a process. Our determinations of the ERE efficiency (Figure 4) suggest that the fraction of neutral SNPs in RN is about 5%, and about 1% in the Orion Nebula. Calculations of the expected charge equilibrium of 3 nm diameter particles in these radiation environments predict distributions with peaks of multiple charge states of two to six positive charges per particle (Bakes & Tielens 1994; Weingartner & Draine 2001). Our own determinations of the lifetime of the ionized state, single or multiple, in RN and in the Orion Nebula (Sect. 3.4) also indicated a likely predominance of multiple positive charge states.

The balance between photoionization and electron capture by ionized nanoparticles in any given environment determines their charge distributions. For a particle of given radius, the resulting charge distribution is almost entirely determined by the parameter $U \frac{\sqrt{T}}{n_e}$ (Bakes & Tielens 1994; Weingartner & Draine 2001). Unfortunately, for most of our ERE sources, there are no independent estimates of the temperature T or the electron density n_e of sufficient reliability to permit a valid examination of the variations of $\lambda_p(ERE)$ and η with $U \frac{\sqrt{T}}{n_e}$. Of the two observed ERE parameters, η represents additional complications, because its value is expected to depend also on the fractional abundance of SNPs relative to larger grains, in addition to the expected dependence on the fraction of SNPs remaining neutral. There is convincing evidence that the abundance of transiently heated particles, i.e. nanoparticles, varies substantially from cloud to cloud (Boulanger et al. 1990). This is in contrast to $\lambda_p(ERE)$, which only depends on the size distribution of the actively luminescent particles, not on their abundance. Therefore, in Figure 8 we employ generic environmental parameters for different ERE source environments to demonstrate the variation of $\lambda_p(ERE)$ with $U \frac{\sqrt{T}}{n_e}$ expected on the basis of our model. The control of the actively luminescent size distribution by photon interactions is different in two separate domains. In the first domain, defined physically by dense dark nebulae (DN) and the diffuse ISM (DISM), increasing photoionization shifts the charge distribution from a predominately neutral state to a state roughly equally divided between neutral particles and singly-charged particles. In this regime, the

ERE peak wavelength is expected to shift towards shorter wavelengths as shown in Figure 8. In the second domain, consisting of reflection nebulae (RN) and HII-regions (HII), particles with two or more positive charges appear. Photofragmentation of the smallest of such particles will rapidly shift the peak of the size distribution to larger sizes, resulting in larger values of $\lambda_p(ERE)$, for the following reasons.

The phase diagram of multiply-charged nanoparticles of a given positive charge state recognizes three possible size ranges (Li et al. 1998). Below a certain critical size, multiply-charged nanoparticles will disintegrate via Coulomb explosion even at 0 K and are thus unstable. Above this critical size, we encounter a range of diameters, where multiply-charged particles are metastable and where fragmentation occurs as a result of Coulomb repulsion and heating to temperatures $0 \text{ K} < T < T_c$, where T_c is the critical temperature, corresponding to the size-dependent boiling temperature of the nanoparticles (Li et al. 1998, eqn. 11). Beyond this metastable size range, particles of a given charge state are stable and can only be vaporized by raising their temperature to $T > T_c$, the same as uncharged particles. Photofragmentation experiments of multiply-charged silicon nanocrystals in the 1 to 6 nm size range (Ehbrecht & Huisken 1999; Bescos et al. 2000) provide strong evidence that doubly and triply ionized silicon particles in this size range are in the metastable regime with respect to photofragmentation. Such particles decay by ejecting small, singly-charged ionic fragments, predominantly Si^+ monomers and Si_2^+ dimers, thus achieving a state of higher stability. However, this decay occurs only during the short interaction with a heating laser photon field and ceases immediately after the particles cool.

Under conditions present in astrophysical ERE sources, where photon fields are relatively diluted, the processes of excitation, ionization, and heating must be considered as sequential, time-separated events, involving single photons. In the diffuse ISM, the smallest stable SNP is a neutral particle which can survive the absorption of a 13.6 eV photon, emit a 2 eV ERE photon, and endure a temperature pulse associated with the addition of 11.6 eV of internal energy. This excess energy can also lead to an ionization, but each successive ionization increases the ionization potential of the particle to (Seidl et al. 1991)

$$I(z, a) = W_b + (2z - 1) \frac{e^2}{2a}, \quad (17)$$

where W_b is the work function of the bulk material and where the second right-hand term represents the additional energy required to remove a further electron from a $(z-1)$ -fold positively charged, conducting sphere of radius a . Photon absorptions by progressively multiply-charged SNPs, which are unable to lose energy via luminescence and which are progressively more difficult to ionize, lead to progressively increased single-photon heating. Recently, Li

& Draine (2001a, 2001c) have calculated the expected temperature distributions of charged pure silicon nanoparticles and of SNPs with SiO_2 mantles. They predict maximum temperatures of ~ 700 K and of ~ 380 K, respectively, for particles of 2 nm diameter in a typical RN environment, such as NGC 2023, where multiple positive charge states would be expected for SNPs (Weingartner & Draine 2001). Particles of twice this diameter reach maximum temperatures of only about half these values under the same conditions.

In the light of these findings, we anticipate, therefore, that multiply charged, metastable SNPs, upon heating by energetic UV photons, achieve a state of increased stability by ejecting singly-charged ionic fragments, thus reducing their overall charge state and mass. This effect will be strongest for the smallest SNPs, which, for a given charge state, experience the highest Coulomb instability and which also gain the highest temperature increase upon absorption of a photon of given energy. The gain in increased stability resulting from the ejection of an ionic fragment is only temporary, however, because a renewed ionization to the previous charge state will leave the now less-massive particle in an even less-stable state. Consequently, in dense radiation fields, the small-size end of an SNP size distribution will be progressively destroyed by a combination of Coulomb explosion and thermal heating. The only particles permanently stable are the larger SNPs, which never reach charge/temperature combinations to place them into the metastable regime for photofragmentation.

4. DISCUSSION

4.1. Limits on the Intrinsic Luminescence Efficiency of Interstellar SNPs

The fit of our model calculations for the SNP quantum yield to the observed lower limits of the ERE luminescence efficiency was achieved by assuming that the intrinsic quantum yield of the SNP ensemble, under conditions present in the diffuse interstellar medium, is about 50%. This number is obtained by having an even balance between neutral SNPs, which have an intrinsic quantum yield of 100%, and ionized SNPs, which do not contribute to the ERE. Quantum yields between 50% and 100% have indeed been found for SNP laboratory samples (Wilson et al. 1993; Credo et al. 1998; Ledoux et al. 2001). It is straightforward to show that the interstellar ERE carrier must have similar efficiencies.

Gordon et al.(1998) estimated that the ERE represents about 3% of the energy of the total dust emission in the high-Galactic-latitude ISM. From a study of diffuse infrared Galactic emission with IRAS, Boulanger & Perault (1988) concluded that about 40% of the Galactic dust emission is attributable to dust grains small enough to undergo significant temperature fluctuations upon absorption of individual photons, which would include nano-sized ERE car-

riers. While cloud-to-cloud variations of this fraction were observed (Boulanger et al. 1990), this general result was confirmed by observations with DIRBE (Dwek et al. 1997; Bernard et al. 1994). A certain fraction, estimated as about 25% of the small-particle emission or about 10% of the total dust emission, is usually attributed to polycyclic aromatic hydrocarbons (PAHs) in order to account for the presence of the so-called unidentified infrared band (UIB) features in the Galactic spectrum (Desert et al. 1990; Dwek et al. 1997; Misselt et al. 2001). If SNPs are the ERE carrier, they would contribute to the remaining small-particle emission component, which amounts to about 30% of the total dust emission, after subtracting the PAH component. Other possible contributors to the small-particle emission are tiny carbonaceous grains and tiny amorphous silicate grains (Li & Draine 2001b).

Given the absorption spectrum of SNPs (Zubko et al. 1999) and the spectrum of the interstellar radiation field (Mathis et al. 1983), a typical photon exciting an SNP has a likely energy of $E_{abs} = 8$ eV, of which about 2 eV would be emitted as ERE, if the SNP is capable of luminescing, and 6 eV would be thermalized by the particle and emitted in the infrared. Let us consider two limiting cases for the intrinsic efficiency of the ERE carrier. The highest value for the quantum yield is 100%, assuming that a single excitation can at most result in a single luminescence photon. Then, three times as much energy as is emitted in form of the ERE is contributed by thermal emission to the IR. With the estimate of Gordon et al.(1998), we find that about 9% of the total dust emission, or about 1/3 of the small particle emission not attributed to PAHs could be resulting from the presence of SNPs in the interstellar dust mixture. Conversely, a lower limit to the intrinsic efficiency of the interstellar ERE carrier, assuming they are nanoparticles, can be obtained by assuming that all the small-particle thermal emission not assigned to PAHs is produced by the ERE carrier. The associated efficiency can then be obtained from (Duley 1992):

$$\frac{ERE}{Thermal} \sim \left(\frac{3\%}{30\%} \right) \sim \left(\frac{\eta \cdot E_{ERE}}{E_{abs} - \eta \cdot E_{ERE}} \right) \quad (18)$$

where E_{ERE} is the bandgap energy of the ERE carrier. The resulting lower limit to the intrinsic efficiency of the ERE carrier is $\eta \geq 36\%$. Since our SNP model equates the intrinsic efficiency of the SNP ensemble with the fraction of neutral SNPs, our assumption of 50% for this fraction is consistent with the observed characteristics of the actual ERE carrier.

4.2. Prediction of the SNP Cross Section for Single-Photon Ionization

An intrinsic quantum yield of $\geq 36\%$ of the ERE carrier in the diffuse ISM implies that the value of P_0 (Eqn. 12) is ≥ 0.36 for the radiation field and the electron recombination rate applicable to that environment. This condition is met provided $\tau \geq 1.8 \tau_i$. Thus, we find:

$$\frac{\tau}{\tau_i} = \left(\frac{\langle \sigma \rangle_i \cdot \int_{5.1\text{eV}}^{13.6\text{eV}} 4\pi J_\nu \frac{d\nu}{h\nu}}{\pi a^2 \cdot \tilde{\sigma} \cdot n_e \cdot v_e \cdot s} \right) \geq 1.8, \quad (19)$$

where $\langle \sigma \rangle_i$ is the average cross section for single-photon ionization, averaged over the energy range from 5.1 eV to 13.6 eV of the interstellar radiation field. Eqn.(19) allows us to evaluate the value of $\langle \sigma \rangle_i$. With a geometric cross section of a typical SNP, $\pi a^2 = 10^{-13} \text{ cm}^2$, $\tilde{\sigma}$, the reduced cross section of Draine & Sutin (1987) estimated at 200, an electron density $n_e = 0.03 \text{ cm}^{-3}$, an average electron speed $v_e = 3 \cdot 10^6 \text{ cm s}^{-1}$, a sticking coefficient $s = 0.3$, and a flux of ionizing photons of $2.9 \cdot 10^8 \text{ cm}^{-2}\text{s}^{-1}$, we find $\langle \sigma \rangle_i \leq 3.4 \cdot 10^{-15} \text{ cm}^2$. A published measurement of this quantity does not exist and our value is, therefore, a specific prediction made by the SNP model which can be used to either confirm or falsify our model. Our prediction applies to SNPs of average diameter 3.5 nm, expected to luminesce with peak emission around a wavelength of $\sim 700 \text{ nm}$ (Ledoux et al. 2000). This ionization cross section is expected to vary with radius a as $\sim a^2$ (see Sect. 3.5).

The photoionization cross section measures the likelihood that the absorption of a single photon with energy above the ionization threshold of SNP's ($\sim 5.1 \text{ eV}$) leads to the ejection of an electron. Experiments conducted with palladium nanoparticles (Schleicher et al. 1993), with sizes and work function comparable to those of SNPs (Fuke et al. 1993), present useful information with which to assess the likelihood that our cross section prediction is reasonable. The absolute photoelectron yield per photon of palladium nanoparticles for photons within 1 eV above the threshold is only of the order of 10^{-2} , and it approaches unity only at a photon energy of $\sim 10 \text{ eV}$. Similar increases in the photoelectric yield per photon by two to three orders of magnitude over the photon energy range from 5 eV to 10 eV have been reported by Burtcher et al. (1984) for small silver and gold particles. Theoretical calculations of the photoelectron yield of small silicate grains by Ballester et al. (1995) predict a yield of only 0.1 at the Lyman limit, decreasing to 0.001 at a photon energy of 8 eV. SNPs more likely will behave like silicates or other insulators, where electron-phonon scattering interferes with the ejection of photoelectrons, rather than like small metal clusters, where electron-electron scattering takes the place of the process by which most of the energy of absorbed photons with energy $E > E_i$ is converted into heat (Gail & Sedlmayr 1980). This suggests, if the cited results are applicable to SNPs, that the photoionization cross section of SNPs is substantially

smaller than the absorption cross section throughout most of the astrophysically relevant UV spectrum. Absorption cross sections measured for SNPs (Kovalev et al. 2000) cover only the photon energy range from 1.48 eV to 3.53 eV and extend from a few 10^{-19} cm² to about 10^{-14} cm², enough to estimate that the absorption cross sections of SNPs of about 3.5 nm diameter are not more than about 10^{-13} cm² in the UV. According to our estimate, the single-photon photoionization cross section of SNPs, then, is not greater than about $3 \cdot 10^{-2}$ times the absorption cross section.

Another way to assess the likely validity of our result is to extrapolate the ionization cross section of SNPs from the ionization cross section of neutral silicon atoms. Near threshold, the latter cross section is about $5 \cdot 10^{-17}$ cm² (Verner et al. 1996). A typical SNP of 3.5 nm diameter has about 800 silicon atoms, with a combined ionization cross section of $4.0 \cdot 10^{-14}$ cm². Our estimate is about one order of magnitude smaller, corresponding to a photoelectron yield of about 0.1. This agrees surprisingly well with the yields found in experiments and in calculations, when averaged over the energy range of photons from 5.1 to 13.6 eV and a spectrum given by that of the interstellar radiation field.

4.3. The Special Role of Lynds 1780

Lynds 1780 (L 1780) is a high-latitude ($b = 36.9^\circ$) dark nebula. Mattila (1979) noted the unusually red color of this object and determined its spectral energy distribution, but given that ERE as a general interstellar phenomenon was not to be recognized for several more years, he failed to find a likely source for the apparent red excess in the spectrum of L 1780. The identification of the red excess with ERE was proposed by Chlewicki & Laureijs (1987), who noted the similarities between the spectra of L 1780 and the Red Rectangle. L 1780 is an optically thick cloud ($A_B \sim 3$ mag) with a density of about 10^3 cm⁻³ (Mattila 1979), exposed to the local ($D \sim 100$ pc) interstellar radiation field.

L 1780 occupies a special role among all ERE sources with likely interstellar dust mixtures: it has the highest efficiency determined so far ($\sim 13\%$; Fig. 4) for an object containing such a dust mixture and it exhibits a very broad emission band with a peak near 700 nm (Fig. 2). Until now, in view of the low density of the exciting radiation field this relatively long peak wavelength made L 1780 appear the odd outlier on graphs such as Figure 2. Our SNP model provides a natural explanation for the seemingly odd characteristics of the ERE in L 1780. In view of the much higher gas density of L 1780 compared to the diffuse interstellar medium in general, the electron density will be higher in L 1780 as well, while the UV-photon density is actually reduced due to the cloud's intrinsic opacity, so that the overall ionization equilibrium tends more towards neutrality. Hence, $\frac{\tau}{\tau_i} \ll 1$ in L 1780, while

$\frac{\tau}{\tau_i} \sim 1$ in the diffuse ISM and $\frac{\tau}{\tau_i} \gg 1$ in reflection nebulae and HII regions. These are the conditions, respectively, under which our model predicts predominantly neutral SNPs, SNPs approximately equally balanced between neutral and ionized, and predominantly ionized SNPs. Thus, in L 1780 the SNPs are more predominantly neutral than is the case in the diffuse ISM. The larger SNPs, which are removed from luminescing in the diffuse ISM due to the size-dependent ionization, are now restored as ERE contributors. Consequently, both the overall quantum efficiency increases and the peak wavelength shifts towards larger values compared to the diffuse ISM. The ERE spectrum of L 1780 may, therefore, be regarded as most closely approximating that of a size distribution of luminescing SNPs, hardly modified by ionization.

4.4. Multiple Ionization and Photofragmentation

In Section 3.5 we have argued that Coulomb explosions of multiply-charged, metastable SNPs will gradually erode the small-size end of an existing SNP size distribution, once it is exposed to dense and hard radiation fields. An observable consequence of such conditions would be the increased gas-phase abundance of Si^+ ions as well as SiO molecules in the photon-dominated regions between dense molecular clouds and nearby hot stars. An impressive example of such an enhanced gas-phase abundance of Si^+ in the presence of a dense radiation field can be found in the ISO observations of the reflection nebula NGC 7023 by Fuente et al. (2000). In the inner cavity of this nebula, where ERE is almost totally absent (Witt & Boroson 1990), at least 20% to 30% of the cosmic abundance of silicon is found in the gas phase, while the inferred gas-phase abundance of silicon drops to about 5% in the high-density ERE filaments to the south and to the north-west of the central B 3 V star, HD 200775. This is consistent with an almost total photodisintegration of all SNPs in this volume, given that the SNP model requires about 20% of the total silicon abundance in the form of SNPs. We suggest that multiple ionization of SNPs and the resulting gradual photofragmentation may have destroyed the SNPs in the inner cavity of NGC 7023. We also suggest that this is the process by which the size distribution of SNPs in regions of high radiation density is changed permanently, so that only the larger SNPs capable of luminescing at longer wavelengths survive.

4.5. Infrared Band Emissions from SNPs

A frequently raised question about interstellar SNPs concerns expectations that SNPs should give rise to infrared band emissions for which there is no clear present evidence. Li

& Draine (2001a, 2001c) made a first attempt at calculating the expected emission spectrum of pure silicon particles and SNPs with oxide coatings. They predict the presence of a relatively sharp emission feature at $16.4 \mu\text{m}$ for pure silicon particles and a still stronger, broad emission peak at $20 \mu\text{m}$ due to SiO_2 for oxide-coated SNPs. Several comments are in order regarding pure silicon particles: i) The case of pure silicon particles appears astrophysically less interesting; ii) such particles, with dangling bonds at the surface remaining unpassivated, would not luminesce in the ERE band; iii) they have never been proposed as the ERE carrier; iv) they would not be expected to be chemically stable under interstellar conditions, if they could form in the first place. In our view, the predicted $16.4 \mu\text{m}$ feature is, therefore, of questionable significance.

Adding an oxide coating to SNPs, according to Li & Draine (2001a), lowers the most likely temperature of the nanoparticles from 300 K to about 75 K, due to the oxide’s ability to radiate strongly in Si-O vibrational bands. This lower temperature, however, prohibits significant emission at the most commonly investigated band near $10 \mu\text{m}$ and leaves the radiation near $20 \mu\text{m}$ as the dominant mode. The detectability of the $20 \mu\text{m}$ band is a function of the SNP abundance as a fraction of the radiating dust mass, and thus is inversely proportional to the intrinsic ERE quantum efficiency of the oxide-covered SNPs. Experimentally determined quantum efficiencies for SNPs are found to be in the range from 50% to 100% (Wilson et al. 1993; Credo et al. 1999; Ledoux et al. 2001). Li & Draine (2001a), from their model calculations, conclude that that even for such high-efficiency SNPs, the predicted intensity of the $20 \mu\text{m}$ band emission from the diffuse ISM exceeds observed upper limits set by DIRBE observations by a factor of 7. Similarly, in the reflection nebula NGC 2023, they find the predicted $20 \mu\text{m}$ feature strength to exceed the observed intensity seen in an ISO spectrum by a significant factor. In order to decide, whether these constraints are in fact as severe as they appear, several objectives would need to be pursued in the future. These include sensitive spectroscopic observations of the $20 \mu\text{m}$ region in ERE sources, experimental determinations of the dielectric functions of oxygen-passivated SNPs for more solidly-based model calculations, as well as controlled oxidization experiments aimed at determining the minimum amount of SiO_2 needed for the effective passivation of SNPs.

Detection of the predicted $20 \mu\text{m}$ emission band would be most likely in objects where the abundance of SNPs exceeds that in the interstellar medium by a wide margin. The Red Rectangle (Schmidt et al. 1980) has an unusually strong ERE band, which suggests that the dust locally produced in this proto-planetary nebula is exceptionally rich in the particles producing the ERE. The publically accessible ISO-SWS spectrum of the Red Rectangle (http://isowww.estec.esa.nl/galleries/cir/red_rect.html) does not exhibit any prominent feature at $20 \mu\text{m}$. However, a detailed analysis of this spectrum has yet to be done. The Red Rectangle is a member of a class of similar objects, bi-polar proto-planetary nebulae

with dust produced by mass-losing AGB stars. Hrivnak et al. (2000) have used ISO to study the infrared spectra of nine such objects. Four of these exhibit a strong emission band at $21\ \mu\text{m}$, closely resembling the profile predicted by Li & Draine (2001a). In two additional objects, the identification of the $21\ \mu\text{m}$ band is tentative; in three objects the band was not detectable. None of these nebulae has been studied for the presence of ERE, and none is expected, because the spectral types of the central stars are much later than that of the illuminating star in the Red Rectangle (B 9.5 III). The possibility that SNPs are formed in protoplanetary nebulae and are excited to emit ERE in the case where central stars with sufficient ultraviolet photons are present, deserves further investigation. There has also been an indication that the $21\ \mu\text{m}$ band is present in the dust emission spectrum of the supernova remnant Cas A (Douvion et al. 2001), which, together with the strong presence of SiO emission from the remnant of SN 1987A (Roche et al. 1991), leads to the suggestion that supernova remnants could be locations for SNP formation. An alternate suggestion for the identification of the $21\ \mu\text{m}$ feature in proto-planetary nebulae has been provided by von Helden et al. (2000), who proposed titanium carbide nanocrystals as the carrier of this feature. No estimates exist on whether the likely abundance of titanium carbide is sufficient to explain the intensity of the $21\ \mu\text{m}$ band.

5. SUMMARY

The existing body of observational data on the interstellar luminescence process known as ERE shows a wide range of variation in three observational characteristics: the band-integrated intensity, the wavelength of peak emission, and the efficiency with which absorbed UV/optical photons are converted into ERE photons. By systematically analysing all suitable ERE observations available so far, we have shown that the common environmental factor driving the variations in these three characteristics is the radiation field density in the different environments, where ERE has been detected. The ERE intensity increases with radiation density roughly linearly, as expected for photoluminescence; the peak of the ERE band shifts from about 610 nm in the diffuse ISM to beyond 800 nm in O-star dominated HII regions; and the photon conversion efficiency is found to be highest in environments with the lowest density of exciting photons, only to decline significantly in denser radiation fields. In the second part of this paper, we have introduced a model for the ERE carrier in which photoionization of nanoparticles, balanced by recombination with free electrons, is the controlling physical process which determines the total fraction of actively luminescing particles. The model relies on experimental findings, showing that ionization will quench photoluminescence in a luminescing semiconductor nanoparticle, with luminescence being restored upon recombination. This model successfully reproduces the observed variations

of the ERE intensity and the ERE photon conversion efficiency for a large range of radiation field densities. We find that under the complete range of conditions where ERE is being observed in astronomical environments, the single-photon ionization process is always dominant over the two-photon Auger ionization process. In dense-radiation environments, photoionization will lead to relatively high positive charge states for SNPs, which will render the smallest SNPs unstable against photofragmentation upon single-photon heating. We suggest this process as the explanation for the observed shift of the wavelength of peak ERE intensity toward larger values in UV-radiation fields of increased density. Silicon nanoparticles have been proposed as carriers of the ERE in view of their ability to match the spectral characteristics of the ERE and the efficiency constraints better than any other current model candidate. In order to match the entire body of ERE data presented in this paper, we require that silicon nanoparticles with an average diameter of 3.5 nm have an ionization cross section of about $3.4 \cdot 10^{-15} \text{ cm}^2$ when exposed to a radiation field with an energy distribution equal to that found in the diffuse ISM of the solar neighborhood. The experimental determination of this cross section would represent a critical test for the model proposed here. Finally, we note that sensitive spectroscopic searches for the 20 μm band predicted to be associated with oxygen-passivated SNPs in ERE-bright interstellar environments would provide severe constraints for the validity of the SNP model, especially if accompanied by experimental efforts to determine the dielectric functions for these particles in the laboratory.

Acknowledgement: We are extremely grateful to Bruce Draine, Friedrich Huisken, Gilles Ledoux, and Aigen Li, who reviewed an earlier version of this paper and who provided much critical input to the present version. We also acknowledge extensive stimulating discussions about ERE and nanoparticles with Louis Brus, Bob Deck, Walt Duley, Minoru Fujii, Dieter Gerlich, Karl Gordon, Thomas Henning, and Daniele Pierini. Finally, we acknowledge again Bruce Draine, who as referee provided further helpful criticism and several very constructive suggestions. This work was supported through Grant NAG5-9202 from the National Aeronautics and Space Administration to The University of Toledo.

REFERENCES

- Bakes, E.L.O., & Tielens, A.G.G.M. 1994, *ApJ*, 427, 822
- Baldwin, J.A. et al. 1996, *ApJ*, 468, L115
- Ballester, J.L., Shi, Y., & Dwek, E. 1995, *J. Opt. Soc. Am. B*, 12, 1211
- Banin, U., Bruchez, M., Alivisatos, A.P., Ha, T., Weiss, S., & Chemia, D.S. 1999, *J. Chem. Phys.*, 110, 1195

- Bernard, J.P., Boulanger, F., Desert, F.X., Giard, M., Helou, G., & Puget, J.L. 1994, *A&A*, 291, L5
- Bescos, B., Hoch, R., Schmidtke, H.-J., & Gerber, G. 2000, *Appl. Phys. B*, 71, 373
- Bohren, C.F., & Huffman, D.R. 1983, *Absorption and Scattering of Light by Small Particles*, (New York: John Wiley & Sons, Inc.)
- Boulanger, F., & Perault, M. 1988, *ApJ*, 330, 964
- Boulanger, F., Falgarone, E., Puget, J.L., & Helou, G. 1990, *ApJ*, 364, 136
- Brongersma, M.L., Kik, P.G., Polman, A., Min, K.S., & Atwater, H.A. 2000, *Appl. Phys. Lett.*, 76, 351
- Burtscher, H., Schmidt-Ott, A., & Siegmann, H.C. 1984, *Z. Phys. B - Cond. Matt.*, 56, 197
- Castro-Carrizo, A., Lucas, R., Bujarrabal, V., Colomer, F., & Alcolea, J. 2001, *A&A*, 368, L34
- Chepic, D.I., Efros, A.L., Ekimov, A.I., Ivanov, M.G., Kharchenko, I.A., Kudriavtsev, I.A., & Yazeva, T.V. 1990, *J. Lumin.* 47, 113
- Chlewicki, G., & Laureijs, R.J. 1987, in *Polycyclic Aromatic Hydrocarbons and Astrophysics*, ed. A. Leger, L. d'Hendecourt, & N. Boccarda, (Dordrecht: Reidel Publ. Co.), NATO ASI Series, Vol. 191, p. 335 - 337
- Credo, G.M., Mason, M.D., & Buratto, S.K. 1999, *Appl. Phys. Lett.*, 74 (14), 1998
- Darbon, S., Perrin, J.-M., & Sivan, J.-P. 1999, *A&A*, 348, 990
- Darbon, S., Savagno, A., Perrin, J.-M., Savine, C., Ducci, V., & Sivan, J.-P. 2000, *A&A*, 364, 723
- Delerue, C., Allan, G., & Lannoo, M. 1993, *Phys. Rev. B*, 48, 11024
- Delerue, C., Allan, G., & Lannoo, M. 1998, *Semiconductors and Semimetals*, 49, 253
- Desert, F.-X., Boulanger, F., & Puget, J.L. 1990, *A&A*, 237, 215
- Douvion, T., Lagage, P.O., & Pantin, E. 2001, *A&A*, 369, 589
- Draine, B.T., & Sutin, B. 1987, *ApJ*, 320, 803
- Duley, W.W. 1985, *MNRAS*, 215, 259
- Duley, W.W. 1992, *MNRAS*, 258, 773
- Dwek, E. et al. 1997, *ApJ*, 475, 565
- Ehbrecht, M., & Huisken, F. 1999, *Phys. Rev. B*, 59, 2975
- Efros, A.L., & Rosen, M. 1997, *Phys. Rev. Lett.*, 78, 1110

- Freedhoff, M.I., & Marchetti, A.P. 1997, in Handbook of Optical Properties. II. Optics of Small Particles, Interfaces, and Surfaces, ed.R.E. Hummel, & P. Wissmann, New York: CRC Press, 1-30
- Fuente, A., Martin-Pintado, J., Rodriguez-Fernandez, N.J., Cernicharo, J., & Gerin, M. 2000, A&A, 354, 1053
- Fujii, M., Mimura, A., Hayashi, S., & Yamamoto, K. 2000, J. Appl. Phys., 87, 1855
- Fuke, K., Tsukamoto, K., Misaizu, F., & Sanekata, M. 1993, J. Chem. Phys., 99, 7807
- Furton, D.G., & Witt, A.N. 1990, ApJ, 364, L45
- Furton, D.G., & Witt, A.N. 1992, ApJ, 386, 587
- Gail, H.-P., & Sedlmayr, E. 1980, A&A, 86, 380
- Gail, H.-P., & Sedlmayr, E. 1999, A&A, 347, 594
- Garray, G., Mardones, D., & Rodriguez, L.F. 2000, ApJ, 545, 861
- Gordon, K.D., Witt, A.N., & Friedmann, B.C. 1998, ApJ, 498, 522
- Gordon, K.D., et al. 2000, ApJ, 544, 859
- Hirano, N., Mikami, H., Umemoto, T., Yamamoto, S., & Taniguchi, Y. 2001, ApJ, 547, 899
- Hrivnak, B.J., Volk, K., & Kwok, S. 2000, ApJ, 535, 275
- Huffman, D.R. 1977, Adv Phys., 29, 129
- Kerr, T.H., Hurst, M.E., Miles, J.R., & Sarre, P.J. 1999, MNRAS, 303, 446
- Kharchenko, V.A., & Rosen, M. 1996, J. Lumin., 70, 158
- Koch, F., Kovalev, D., Averboukh, B., Polisski, G., & Ben-Chorin, M. 1996, J. Lumin. 70, 320
- Kovalev, D., Diener, J., Heckler, H., Polisski, G., Kuenzner, N., & Koch, F. 2000a, Phys. Rev. B, 61, 4485
- Kovalev, D., Heckler, H., Ben-Chorin, M., Polisski, G., Schwartzkopff, M., & Koch, F. 2000b, J. Porous Mat., 7, 85
- Kurucz, R.L., Peytremann, E., & Avrett, E.H. 1974, Blanketed Model Atmospheres of Early-Type Stars, (Washington, DC: Smithsonian Institution)
- Leach, S. 1986, J. Elect. Spectr. and Related Phenom., 41, 427
- Ledoux, G., Guillois, O., Porterat, D., Renaud, C., Huisken, F., Kohn, B., & Paillard, V. 2000, Phys. Rev. B, 62 (23), 15942
- Ledoux, G., Guillois, O., Huisken, F., Kohn, B., Porterat, D., & Reynaud, C. 2001, A&A, in press

- Li, A., & Draine, B.T. 2001a, ApJ, in press
- Li, A., & Draine, B.T. 2001b, ApJ, 554, 778
- Li, A., & Draine, B.T. 2001c, <http://xxx.lanl.gov/abs/astro-ph/0012509v2>
- Li, Y., Blaisten-Barojas, E., & Papaconstantopoulos, D.A. 1998, Phys. Rev. B, 57, 15519
- Mason, M.D., Credo, G.M., Weston, K.D., & Buratto, S.K. 1998, Phys. Rev. Lett., 80, 5405
- Mathis, J.S., Mezger, P.G., & Panagia, N. 1983, A&A, 128, 212
- Mattila, K. 1979, A&A, 78, 253
- Meyer, B.K., Hofmann, D.M., Stadler, W., Petrova-Koch, V., Koch, F., Omling, P., & Emanuelsson, P. 1993, Appl. Phys. Lett., 63, 2120
- Misselt, K.A., Gordon, K.D., Clayton, G.C., & Wolff, M.J. 2001, ApJ, 551, 277
- Murakami, K., Suzuki, T., Makimura, T., & Tamura, M. 1999, Appl. Phys. A, 69, S13
- Nirmal, M., & Brus, L. 1999, Acc. Chem. Res. 32, 407
- Nirmal, M., Dabbousi, B.O., Bawendi, M.G., Macklin, J.J., Trautman, J.K., Harris, T.D., & Brus, L.E. 1996, Nature, 383, 802
- Perrin, J.-M., & Sivan, J.-P. 1992, A&A, 255, 271
- Rietmeijer, F.J.M., Nuth III, J.A., & Karner, J.M. 1999, ApJ, 527, 395
- Rinnert, H., Vergnat, M., & Marchal, G. 1998, Appl. Phys. Lett., 72, 3157
- Rinnert, H., Vergnat, M., Marchal, G., & Burneau, A. 1999, J. Lumin., 80, 445
- Roche, P.F., Aitken, D.K., & Smith, C.H. 1991, MNRAS, 252, 39
- Rouan, D., Lecoupanec, P., & Leger, A. 1995, Newsletter on Analysis of Astronomical Spectra, 22, 37
- Rubin, R.H., Martin, P.G., Dufour, R.J., Ferland, G.J., Baldwin, J.A., Hester, J.J., & Walter, D.K. 1998, ApJ, 495, 891
- Russell, R.W., Soifer, B.T., & Willner, S.P. 1978, ApJ, 220, 568
- Sakata, A., Wada, S., Narisawa, T., Asano, Y., Iijima, Y., Onaka, T., & Tokunaga, A.T. 1992, ApJ, 393, L83
- Schleicher, B., Burtscher, H., & Siegmann, H.C. 1993, Appl. Phys. Lett., 63, 1191
- Schmidt, G.D., Cohen, M., & Margon, B. 1980, ApJ, L133
- Schmidt, G.D., & Witt, A.N. 1991, ApJ, 383, 698
- Seahra, S.S., & Duley, W.W. 1999, ApJ, 520, 719

- Seidl, M., Meiwes-Broer, K.-H., & Brack, M. 1991, *J. Chem. Phys.*, 95, 1295
- Sitko, M.L., Savage, B.D., & Meade, M.R. 1981, *ApJ*, 246, 161
- Sivan, J.-P., & Perrin, J.-M. 1993, *ApJ*, 404, 258
- Smith, T.L. 2000, Ph.D. Thesis, The University of Toledo
- Snow, T.P., & Witt, A.N. 1996, *ApJ*, 468, L65
- Spitzer, L. 1978, *Physical Processes in the Interstellar Medium*, (New York: John Wiley & Sons)
- Szomoru, A., & Guhathakurta, P. 1998, *ApJ*, 494, L93
- Takeoka, S., Fujii, M., & Hayashi, S. 2000, *Phys. Rev. B*, 62 (24), 16820
- Theiss, W. 1997, *Surf. Sci. Rep.*, 29, 91
- Verner, D.A., Ferland, G.J., & Korista, K.T. 1996, *ApJ*, 465, 487
- Vinciguerra, V., Franzo, G., Priolo, F., Iacona, F., & Spinella, C. 2000, *J. Appl. Phys.*, 87, 8165
- von Helden, G., Tielens, A.C.G.M., van Heijnsbergen, D., Duncan, M.A., Hony, S., Waters, L.B.F.M., & Meijer, G. 2000, *Science*, 288, 313
- Wang, C., Shim, M., & Guyot-Sionnest, P. 2001, *Science*, 291, 2390
- Weingartner, J.C., & Draine, B.T. 2001, *ApJS*, 134, 263
- Waters, L.B.F.M. et al. 1998, *Nature*, 391, 868
- Whittet, D.C.B. 1992, *Dust in the Galactic Environment*, (Bristol: IOP Publishing Ltd.)
- Wilson, W.L., Szajowski, P.F., & Brus, L.E. 1993, *Science*, 262, 1242
- Witt, A.N., & Boroson, T.A. 1990, *ApJ*, 355, 182
- Witt, A.N., & Gordon, K.D. 2000, *ApJ*, 528, 799
- Witt, A.N., & Rogers, C. 1991, *PASP*, 103, 415
- Witt, A.N., & Schild, R.E. 1985, *ApJ*, 294, 225
- Witt, A.N., & Schild, R.E. 1986, *ApJS*, 62, 839
- Witt, A.N., Gordon, K.D., & Furton, D.G. 1998, *ApJ*, 501, L111
- Wolkin, M.V., Jorne, J., Fauchet, P.M., Allan, G., & Delerue, C. 1999, *PRL*, 82, 197
- Zhang, Q., Ho, P.T.P., & Wright, M.C.H. 2000, *AJ*, 119, 1345
- Zubko, V., Smith, T.L., & Witt, A.N. 1999, *ApJ*, 511, L57

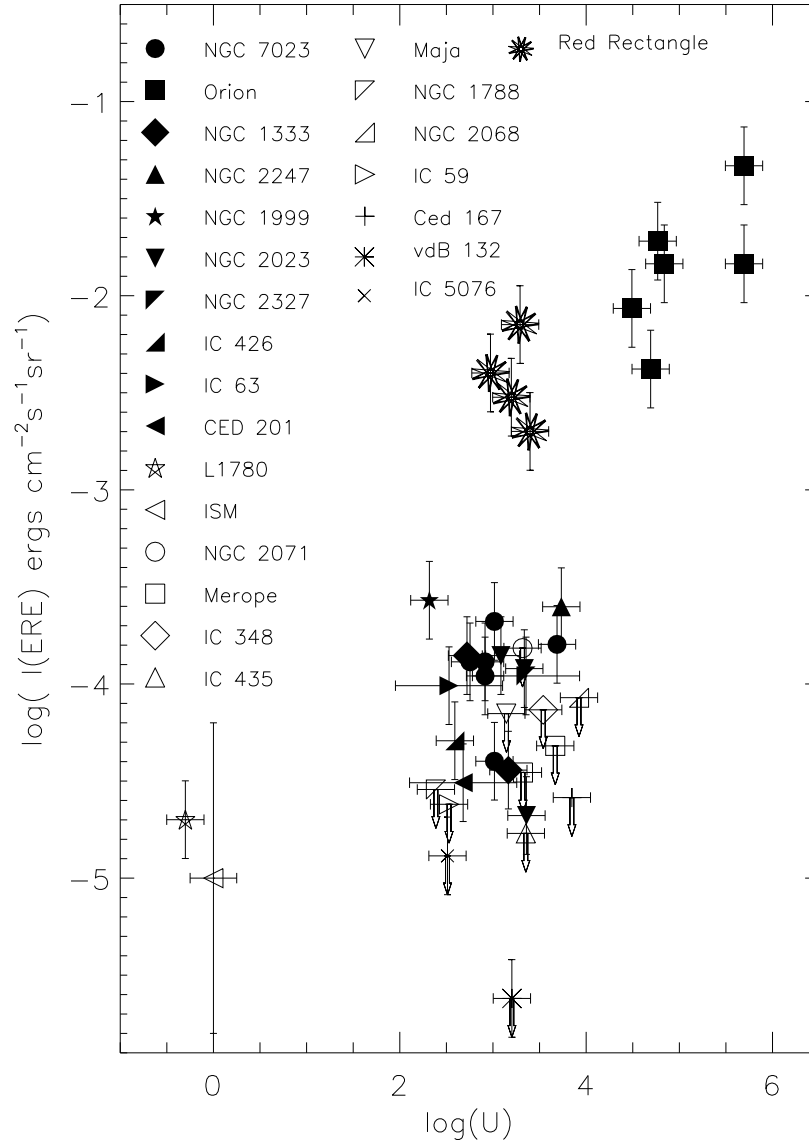


Fig. 1.— The relationship between the ERE intensity and the density of the radiation field in a variety of ERE sources. Downward pointing arrows mark measured upper limits in ERE intensities.

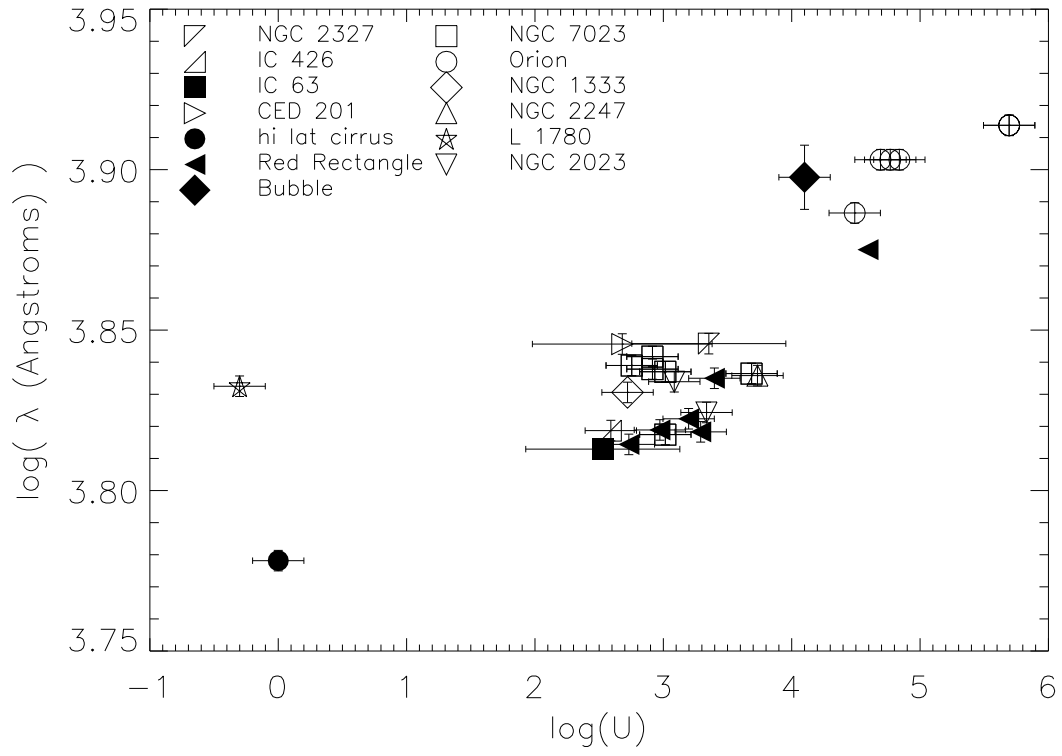


Fig. 2.— The peak wavelength of ERE plotted as a function of radiation field density.

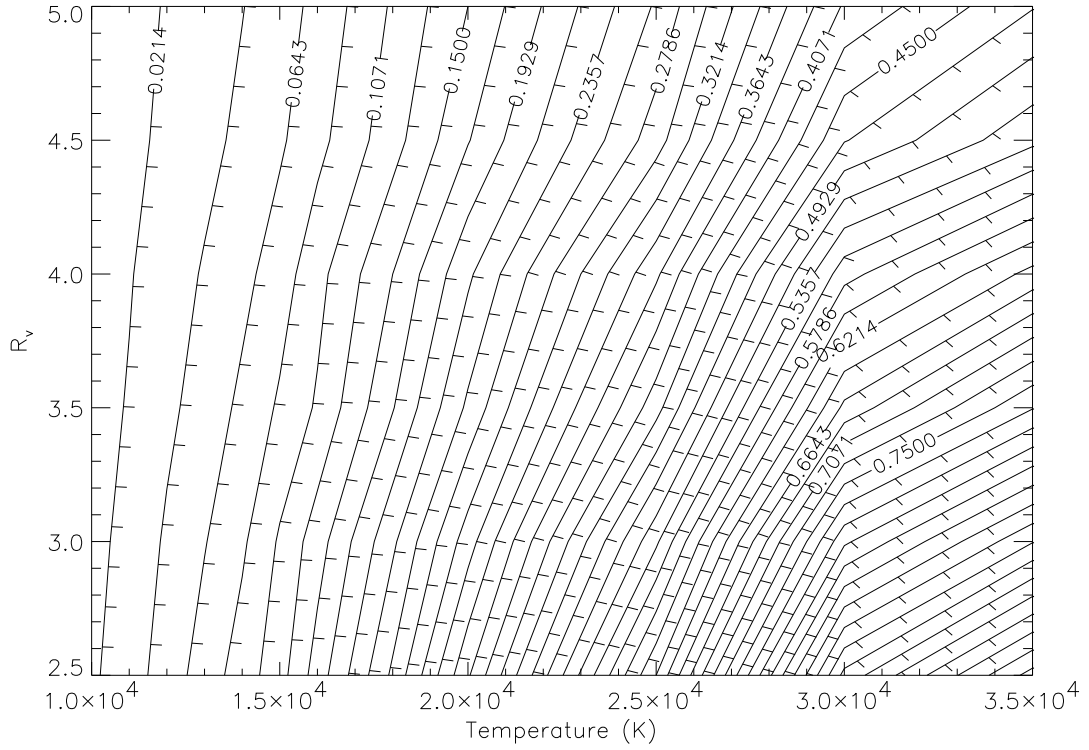


Fig. 3.— A contour diagram showing $I_{ERE}/I_{sca}(band)$ as a function of star temperature and R_V for a UV albedo $a_{UV} = 0.6$, and for an assumed ERE efficiency of 1%.

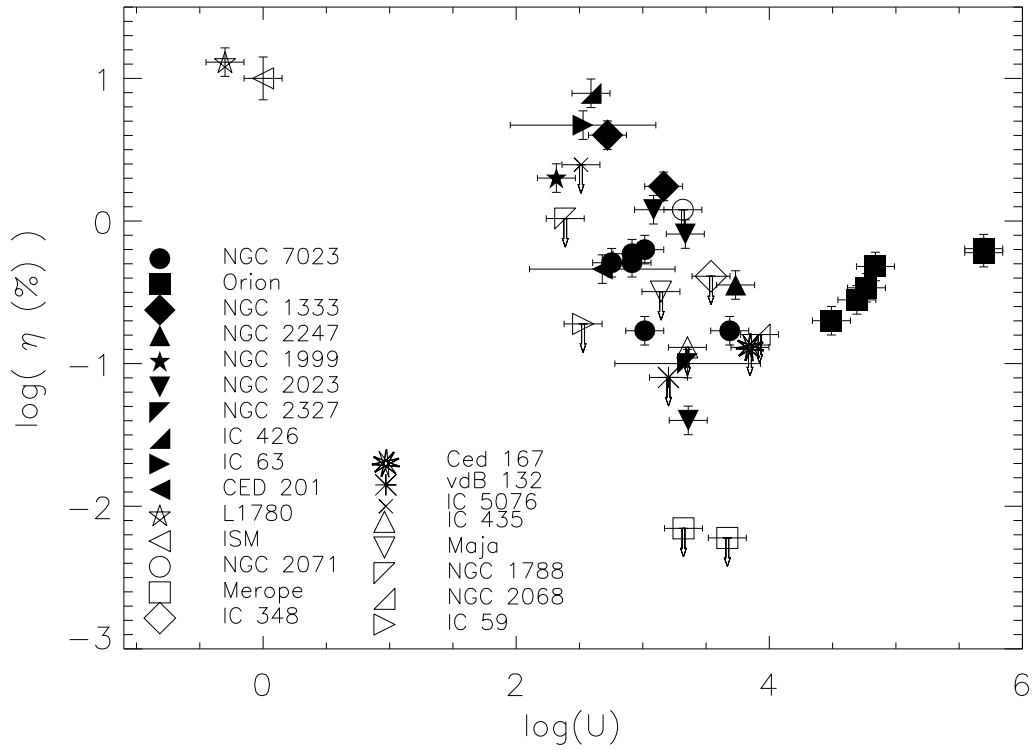


Fig. 4.— The ERE efficiency for a variety of sources plotted as a function of the radiation field density. Both detections and upper limits are included.

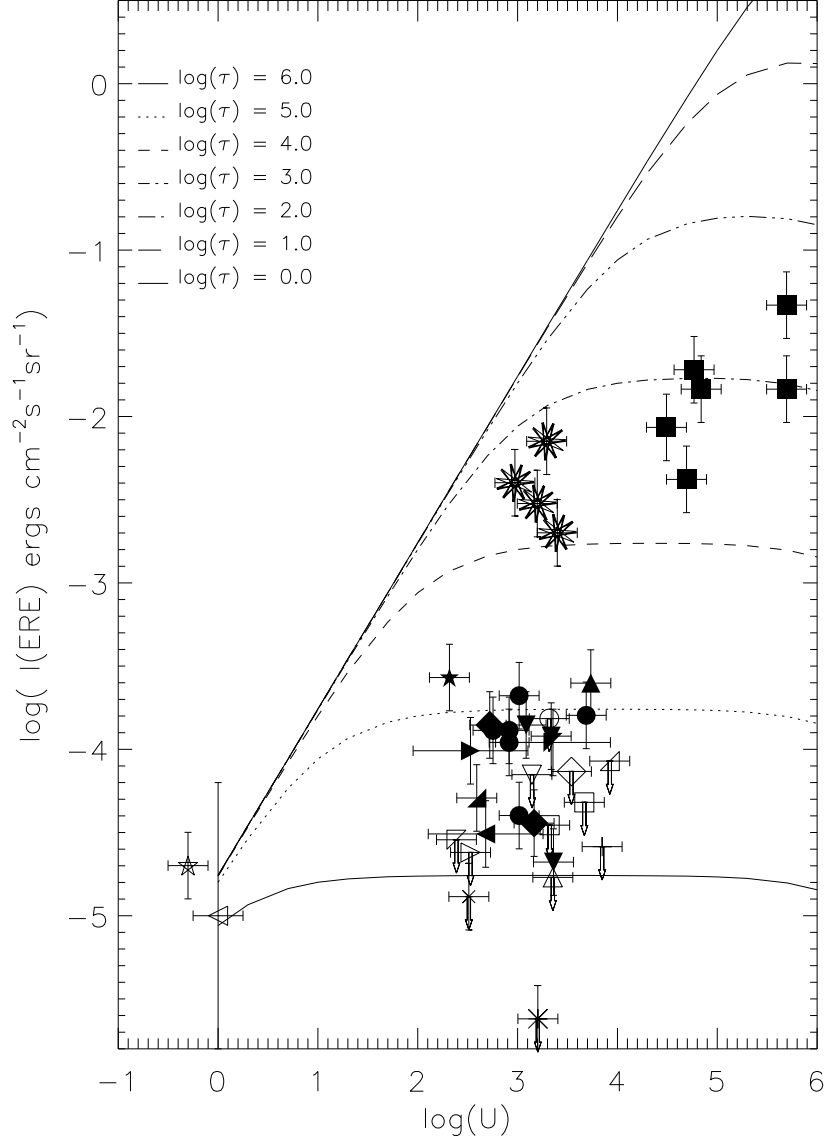


Fig. 5.— The probability P_1 as a function of radiation field density, superimposed upon our ERE intensity data compiled in Section 2. The variable parameter τ measures the lifetime of a SNP in the ionized state in seconds.

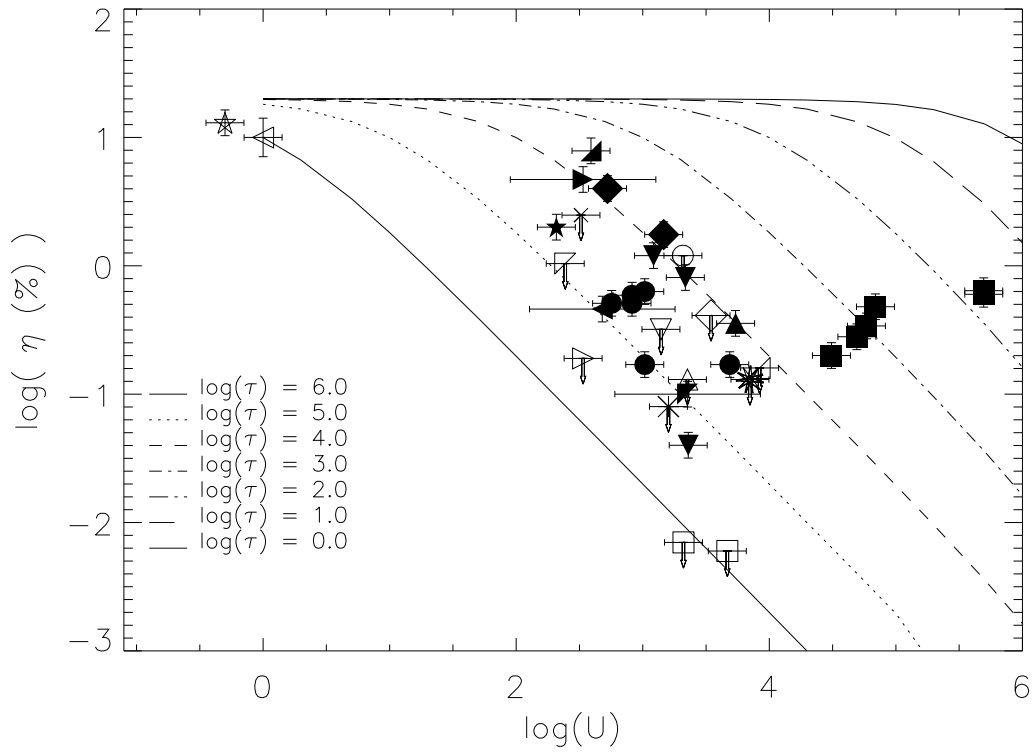


Fig. 6.— The probability P_0 plotted as a function of the radiation field density, superimposed upon the efficiency estimates of Section 2.

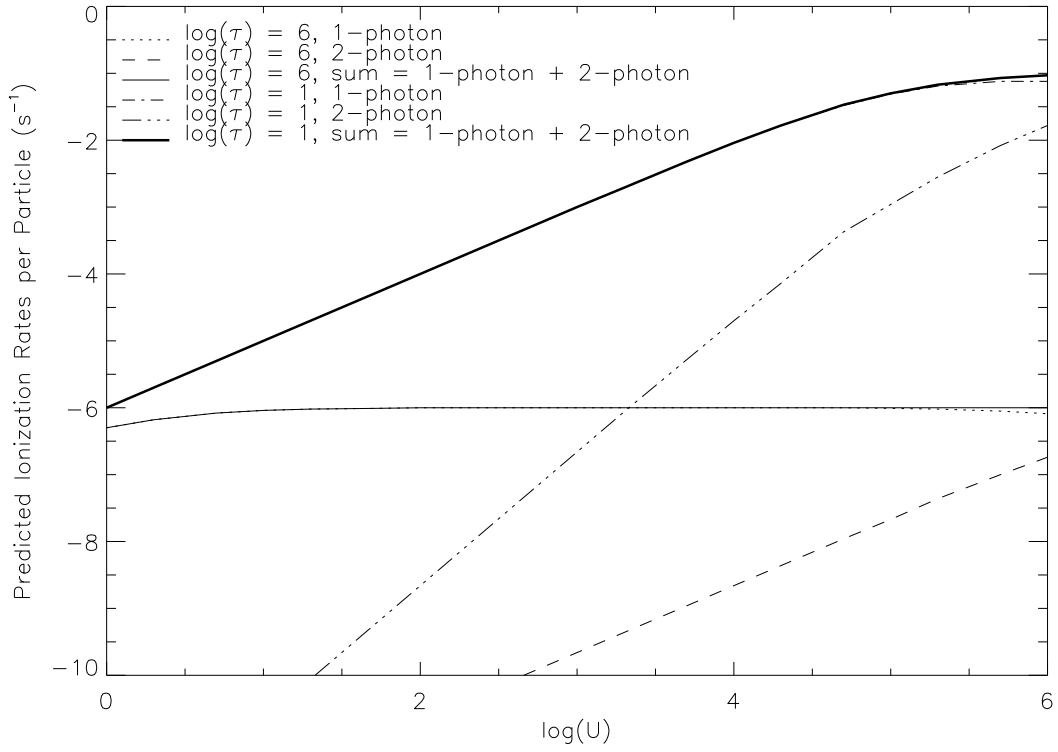


Fig. 7.— The predicted ionization rates per SNP plotted as a function of the radiation field density. Two extreme cases for low and high neutralization rates are shown.

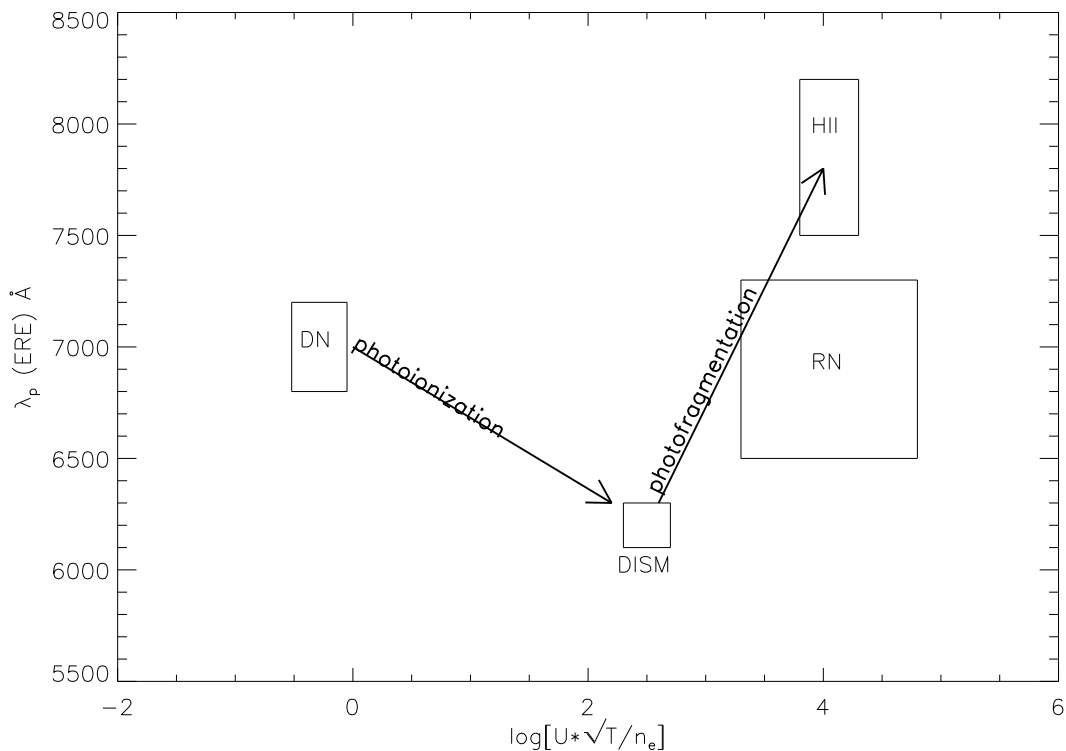


Fig. 8.— The ERE peak wavelengths, as observed in high-latitude dark nebulae (DN), in the diffuse interstellar medium (DISM), reflection nebulae (RN), and HII-regions, are plotted against the parameter $U \frac{\sqrt{T}}{n_e}$, which largely determines the distribution of the carriers over positive charge states. The actively luminescent portion of the size distribution of ERE carriers is first shifted towards smaller sizes by photoionization affecting predominantly the larger particles, then towards larger sizes by photofragmentation, which destroys smaller particles first.